Flexigami: Folded Polygonal Unit Cells For Deployable Metamaterials and Mechanisms

by

Nigamaa Nayakanti

B.Tech., Indian Institute of Technology, Madras (2014)
M.Tech., Indian Institute of Technology, Madras (2014)

Submitted to the Department of Mechanical Engineering
in partial fulfillment of the requirements for the degree of

Master of Science in Mechanical Engineering

at the

MASSACHUSETTS INSTITUTE OF TECHNOLOGY

June 2016

Author ..... Signature redacted
Department of Mechanical Engineering
May 20, 2016

Certified by ..... Signature redacted
Anastasios John Hart
Associate Professor of Mechanical Engineering
Professor in Contemporary Technology
Thesis Supervisor

Accepted by ..... Signature redacted
Rohan Abeyaratne
Chairman, Department Committee on Graduate Theses

Flexigami: Folded Polygonal Unit Cells For Deployable Metamaterials and Mechanisms

by

Nigamaa Nayakanti

Submitted to the Department of Mechanical Engineering
on May 20, 2016, in partial fulfillment of the
requirements for the degree of
Master of Science in Mechanical Engineering

Abstract

Deployable and transformable structures are of broad interest for applications including satellites and space exploration, temporary shelters, packaging, transportation, robotics and medical devices. One emerging approach to scalable fabrication of such structures involves the general concept of Origami-inspired design along with cutting, folding, and fastening of sheet materials. However, contrasting the classical approach of modeling Origami structures as having perfect hinges and rigid panels, consideration of the finite bending and rotational stiffness of these elements is essential to understand their constituent mechanics. Moreover, meta-materials and functional structures having fundamentally new mechanical properties can be designed this way. We present the design, fabrication and mechanics of a novel, deployable cellular material, which we call *Flexigami*. The unit cell takes the form of two parallel regular polygons, connected by a circuit of diagonally creased panels. Upon compression, individual unit cells transform either gently or abruptly between two stable equilibrium states depending on the interplay between hinge and panel properties. The mechanical behavior of each unit cell can be deterministically designed via geometry, dimensions and topology of the panels and hinges. Individual unit cells can collapsed reversible to less than 10% of their deployed volume. Within this transition regime, the force-displacement curve of each cell can be tuned to exhibit a smooth compression behavior or an instability followed by a self-reinforcing response. We use finite-element models complemented by analytical and computational analysis of the results to understand the importance of different mechanical properties of constituent hinges and panels and also demonstrate the fabrication of flexigami cells and mechanisms in various structural materials. Finally we present different mechanisms and their subsequent applications.

Thesis Supervisor: Anastasios John Hart
Title: Associate Professor of Mechanical Engineering
Professor in Contemporary Technology

Acknowledgments

I dedicate this section to everyone who gave me their unyielding support and encouragement throughout my time at MIT. Graduate studies for the past couple of years have been incredibly rewarding experience both personally and professionally. It is a privilege to be part of the dynamic environment offered by MIT. I owe my sincere thanks to many for making this thesis possible and for making my time wonderful. I would like to thank

- Prof. John Hart for his unparalleled guidance, coupled to infinite reservoirs of knowledge and patience which has defined my research experience at MIT. Thank you for all the guidance and pushing me to think deeply.
- NSF Emerging Frontiers in Research and Innovation (EFRI- ODISSEI) for funding research topic of this thesis.
- Fellow members of the Mechanosynthesis Research Group: Abhinav, Dr. Sanha Kim and many others for fruitful discussions and continued support.
- Many friends at MIT and outside, especially Damini and Vennela, for their cheer, compassion and camaraderie. I am endlessly grateful to them.
- Last and most of all, my wonderful family - my mother Manjula Vani, my father Thirupalaiah and my brother Nishanth. I owe everything I am to them

THIS PAGE INTENTIONALLY LEFT BLANK

Contents

List of Figures

List of Tables

THIS PAGE INTENTIONALLY LEFT BLANK

Chapter 1

Introduction

1.1 Background and Motivation

Folding and flexing of thin materials, and their assembly into transformable structures offers opportunity to engineer new capabilities in robotics ([6], [16], [3], [19]), space structures ([33],[25],[27]), and in soft and lightweight actuators ([23],[34],[12],[21],[28]). Capabilities such as multi-stability, deployability, and weight-efficient motion transmission are important to these applications but are often cumbersome to achieve using traditional mechanisms comprising of discrete mechanical components. Therefore, mechanical instabilities arising either from induced defects ([7],[29],[34],[2],[18]) in the material or by prescribing geometrical constraints ([19],[14],[17],[35]) to a structure are of growing interest as a new way of engineering multi-functional materials and structures.

Origami is one way of defining these geometrical constraints in a methodical way. Once a crease pattern is defined in a plane, sequential folding along these creases results in the desired final three dimensional form. Traditional rigid Origami assumes behavior of the structure along a fold line to be that of an ideal hinge with zero rotational stiffness and panels connecting these hinges to be perfectly rigid . Though there are useful applications demonstrated in the literature with these assumptions([8],[26],[24]), Silverberg et.al. in his article [30] rightly points out that the missing piece of phenomenology is that the real materials do in fact bend. In

this article they explored the mechanics of a single unit from the square-twist origami tessellation and concluded that there exists hidden degrees of freedom from face bending which results in non-trivial origami structures. Through subsequent studies ([5]), it is understood that such configurations of a structure are consequences of fundamental incompatibility between the geometry of the predefined folds and non-planar deformations of otherwise assumed rigid panels.

An equilibrium configuration of a folded structure can thereby be reached by minimizing total energy of the system consisting of bending energy of the panels and the energy at the crease. One of the simplest demonstration of this principle consists of a square twist ([31]), where otherwise assumed rigid panels bend and propel its transition between the two stable configurations.

There have been many studies on rigidly foldable cylinders. Early studies include that of Nojima ([20]) where folding patterns were devised on thin flat membrane by modifying traditional Muira-Ori pattern resulting in spiral configurations (Figure. 1-1).

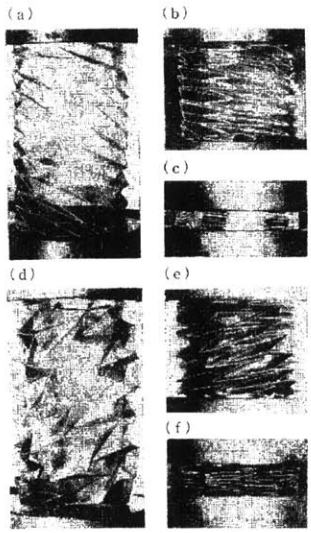

Figure 1-1: Folding process of polypropylene thin circular tubes

Recent works include that of Tachi et.al., [32] where they introduce the concept of rigid-foldable collapsible cellular structure and present geometry of these families of collapsible (Figure. 1-2) cylindrical and cellular structures. Thin walled foldable

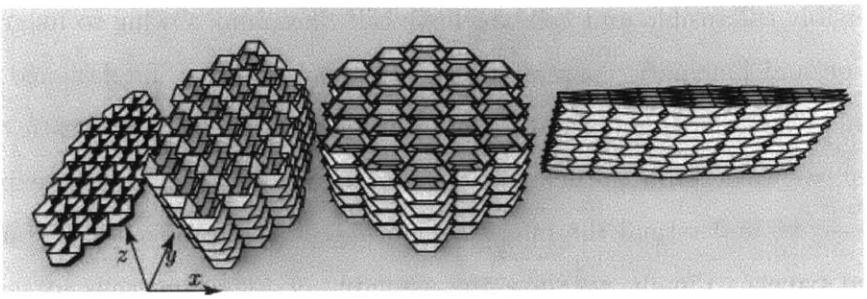

Figure 1-2: Tessellation of a cylinder to produce a one DOF bi-directionally flat-foldable cellylar structure

cylindrical structures can also be generated from 'Kresling' pattern. Initial works on this pattern was by S.D. Guest and S. Pellegrino ([9] & [10]) where they concentrated on developing a numerical model and designing experiments to test a type of foldable cylindrical structure which consisted of triangular panels on a helical strip (Figure. 1-3). In this work, triangulated cylinder is modeled as a simple pin-jointed truss and the plate thickness is neglected and assumes creases offer no resistance to folding.

Figure 1-3: Folding sequence of triangulated cylinders from the work of S.D. Guest and S. Pellegrino [9]

More sophisticated understanding of this structure is presented in [11], where the authors discussed the bistable behavior of the cylinder analytically which was not addressed in previous studies. But, all the analyses is based on the truss model of the cylindrical shell.

This thesis is the study of mechanics of a folded unit cell whose geometry is similar to the kresling pattern, yet features cuts between each adjacent pair of triangles around the outer surface of the cylinder. It represents a novel principle for a fold-

able, reversibly collapsible unit cell which we call *Flexigami*. Owing to its geometric construction and kinematic constraints, the *Flexigami* cell can be designed to have mechanical behavior spanning from that of a soft spring, to reversible elastic collapse. In what follows we describe the geometry and mechanics of the material as explored at the macro-scale, understand the importance of mechanical properties of constituent hinges and panels. Finally we show the assembly of *Flexigami* cells in series and parallel gives rise to multi-stable force-displacement responses, and demonstrate a rotary-linear actuator using *Flexigami* coupled with an accordion bellows.

1.2 Thesis Outline

Chapter 2: presents the geometrical construction of a unit *Flexigami* cell. It details the importance of each of the geometrical parameter in shaping the overall behavior of a unit cell.

Chapter 3: presents a numerical model of a *Flexigami* cell and develop insights into the energetics of the system in a compression cycle and contributions from individual structural elements.

Chapter 4: presents force-displacement responses of *Flexigami* cells to uni-axial compression tension cyclic tests which are displacement controlled.

Chapter 5: presents the finite element model of a seven sided *Flexigami* unit cell and details the contribution of each of the structural element to the overall behavior of *Flexigami*.

Chapter 6: presents the role of different boundary conditions and their effects on the response of a unit cell. We also explore the behavior of the *Flexigami* cells when tiled in series and in parallel. Finally we present mechanisms for compact storage and deployment of space structures made possible with *Flexigami* cells.

Chapter 7: summarizes findings of the thesis and presents key areas of extending the current work.

Chapter 2

Geometry And Construction

A *Flexigami* unit cell is constructed from a N-sided polygon surrounded by diagonally creased parallelograms, and can be cut from a single sheet of stock material (Figures2-1). The cell geometry is defined by the geometric parameters of the regular polygon prescribed by such an arrangement: the number of sides of the polygon **N**, its side length **L**, and a planar angular fraction λ. Each parallelogram is divided into a pair of triangles by a diagonal crease which will be folded to form a valley fold(red line, Fig.2-1). Blue lines denote common edge between either of the polygons and a parallelogram and will be folded to form a mountain fold.

This chapter details the geometrical constraints imposed on a *Flexigami* unit cell which results in the observed behavior and also the coupling between different kinematic quantities.

2.1 Geometrical Constraints and Kinematic Coupling

The unit cell is formed by sequentially folding the planar pattern along the creases indicated. As discussed later, individual rigidity of these creases influence the structural mechanics of a unit cell; in the present case of folded paper, the creases are perforated when the sheet is cut into the unit cell pattern.

To further understand the coupling between the geometry and mechanics of *Flexigami* cell, we first define the geometric constraints that are imposed in the stress-free

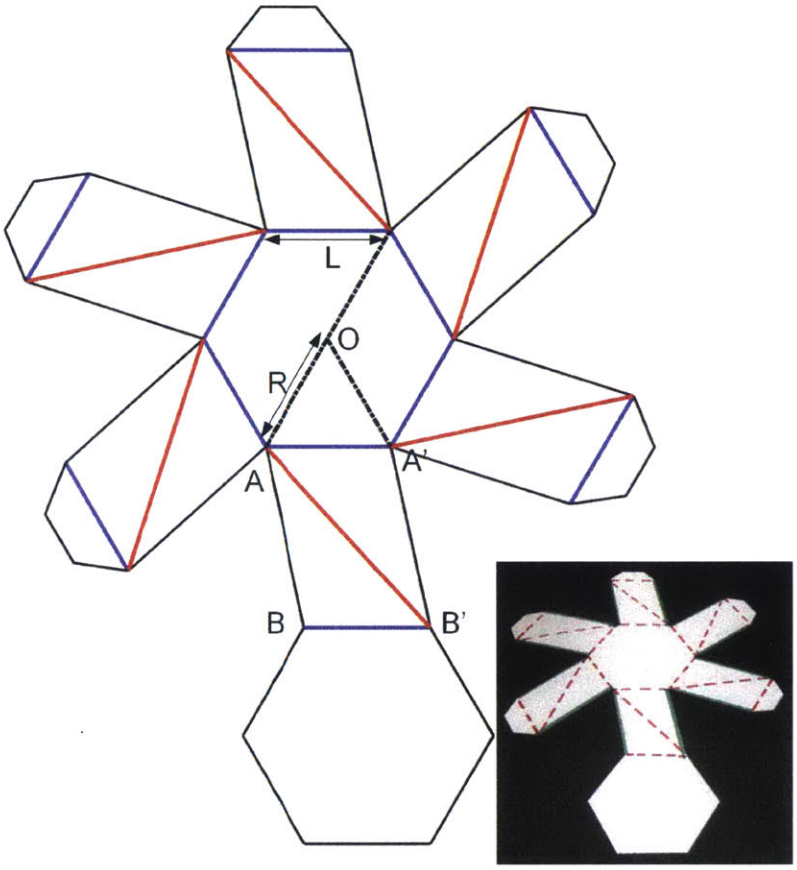

Figure 2-1: **a**: Flexigami unit cell is shown with edges marked in black. red lines indicate Type I creases which are valley folds while blue lines indicate Type II creases which are mountain folds. **b**: photograph of un-folded Flexigami unit cell with $N = 6$, $\lambda = 0.8$ **c**: Photograph of a folded Flexigami unit cell showing out of plane deformations.

folded state

1. The top and bottom panels remain planar and are only permitted to rotate about the vertical (Z) axis.

2. Diagonal creases folded to form valley folds are restricted to remain straight and their lengths are preserved.

3. Free edges of triangular panels (AA', BB') can assume any three-dimensional form, subject to the geometrical constraint of preserving its free length as all the surfaces are considered to be developable.

In the folded yet fully open, stress-free configuration, circum-radius (R), diagonal crease length (ξ), and area of the triangle (ζ) formed by joining the three points $AA'B'$ or ABB' are given by

$$R = 2\frac{1}{L}\cos\left[\frac{\pi(N-2)}{2N}\right]$$

$$\xi = 2R\cos\left[(1-\lambda)\frac{\pi(N-2)}{2N}\right] \tag{2.1}$$

$$\zeta = 4R^2\cos\left[\frac{\pi(\mathrm{N}-2)}{2\mathrm{N}}\right]\cos\left[(1-\lambda)\frac{\pi(\mathrm{N}-2)}{2\mathrm{N}}\right]\sin\left[\lambda\frac{\pi(\mathrm{N}-2)}{2\mathrm{N}}\right]$$

2.2 Variation in γ

Upon compression of the cell, the unconstrained top polygon rotates while being parallel to the bottom polygon, and the triangular panels must bend to accommodate the change in ζ while respecting the geometric constraints described above. Deviation of triangular panels geometry from being plane is quantitatively expressed as fractional change (γ) of the geometrical quantity ζ

$$\gamma = \frac{\zeta_0 - \zeta_i}{\zeta_0}; \tag{2.2}$$

where, ζ_i : instantaneous area of the triangle $AA'B'$ or ABB' and ζ_0 : Initial area of the triangle $AA'B'$ or ABB'

Figure. 2-3 depicts this variation for various values of λ, when $N = 7$, $L = 30$. Here we observe that the change in γ for all values of λ is symmetric with respect to the relative height of a unit cell during compression. We can also state that for lower values of λ ($\lambda \leq 0.5$), γ is less pronounced as compared to γ at higher values of λ. But, as λ increases, we see that γ exhibits a clear global maximum (γ_{max}),

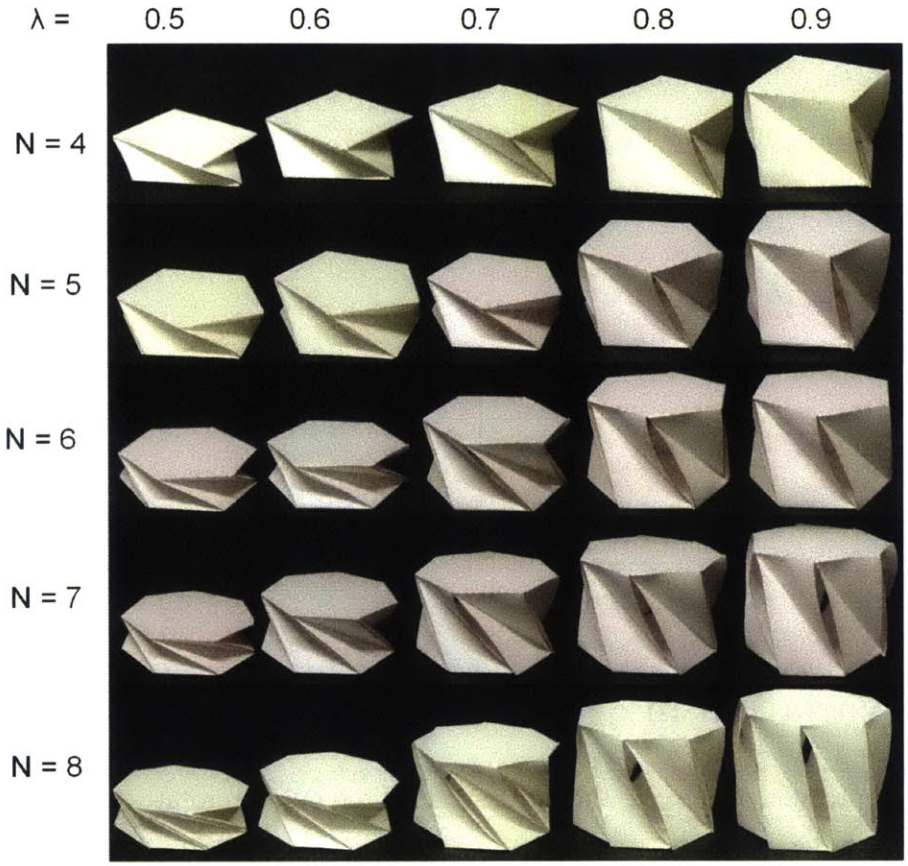

Figure 2-2: Array of Flexigami cells. Each row represents unit cells with the same N and different $\lambda's$ corresponding to $\lambda = 0.5,\ 0.6,\ 0.7,\ 0.8,\ 0.9$. First row represents Flexigami cells with $N = 4$, second row: $N = 5$, third row: $N = 6$, fourth row: $N = 7$, fifth row: $N = 8$.

which increases monotonically with λ. Therefore, upon compression of a *Flexigami* cell, the fractional change in the planar triangular area (γ) is accommodated by the out of plane deformation of the panels. Hence, for a given N, L, the force required to compress the unit cell (hence, its stiffness and peak force when bistable) increases with λ. Now, if λ, L are kept constant and change N (Figure. 2-5), surprisingly we see that γ_{max} decreases with N, suggesting that the force required to compress the cell decreases with N.

As the deformations are symmetric with respect to the relative height of a unit cell during compression, so is the force required to compress the cell. Again, quali-

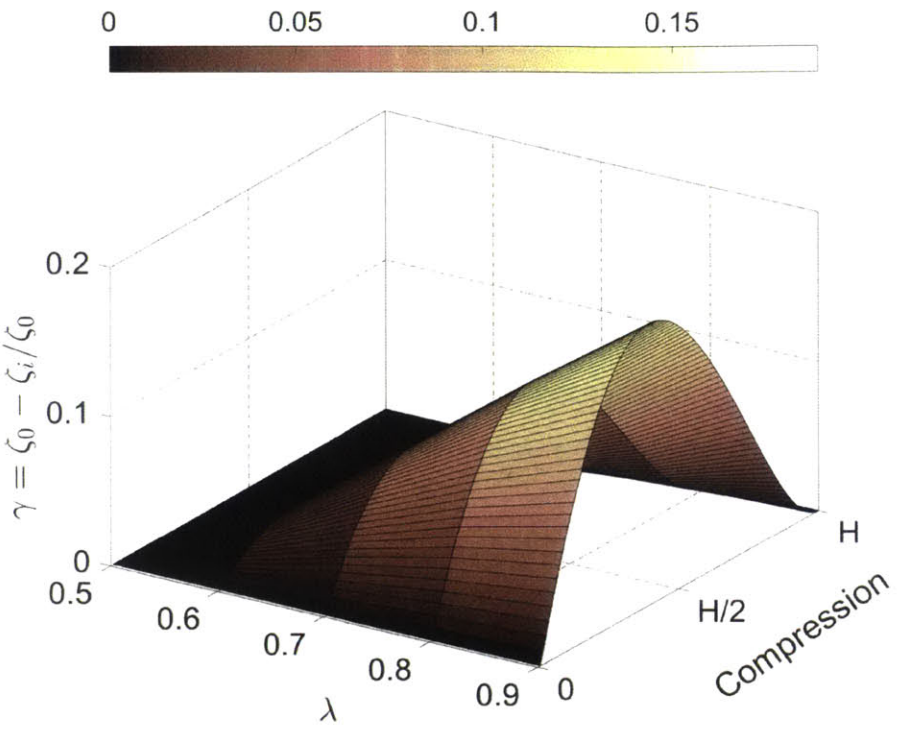

Figure 2-3: **Variation in γ with λ in a compression cycle.** γ is symmetric with respect to half the height of a unit cell in a compression cycle. Variation in γ becomes more pronounced with increasing value of λ.

tatively we can suggest that the force-displacement response of *Flexigami* cell should resemble a bell shaped curve with clear global maximum. As the defined geometrical quantities and kinematic constraints are satisfied in exactly two configurations corresponding to completely opened and closed states, the existence of any intermediate configurations requires material deformations, revealing hidden degrees of freedom of the *Flexigami* cell arising from the finite bending and rotational stiffness of panels and hinges respectively.

It is also important to understand how *gamma* changes when λ and L are kep constant while changing N. Figure. 2-4 represents this variation for $\lambda = 0.9$, $L =$ 30mm and we change N from 4 to 8. As we have considered very high value of λ we see the full development of the barrier in γ in a compression cycle. The peak value of γ - γ_{max} decreases with increasing N suggesting strong snapping or bi-stable nature

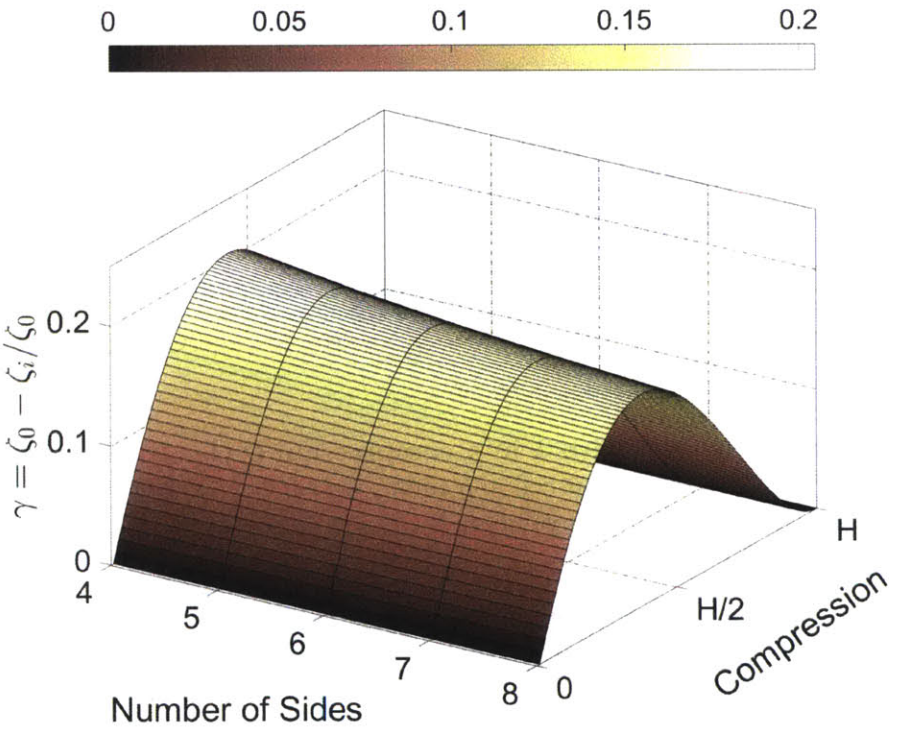

Figure 2-4: **Variation in γ with N in a compression cycle.** γ is symmetric with respect to half the height of a unit cell in a compression cycle. γ_{max} decreases with increasing value of N

for lower values of N rest being the same.

2.3 Variation in θ

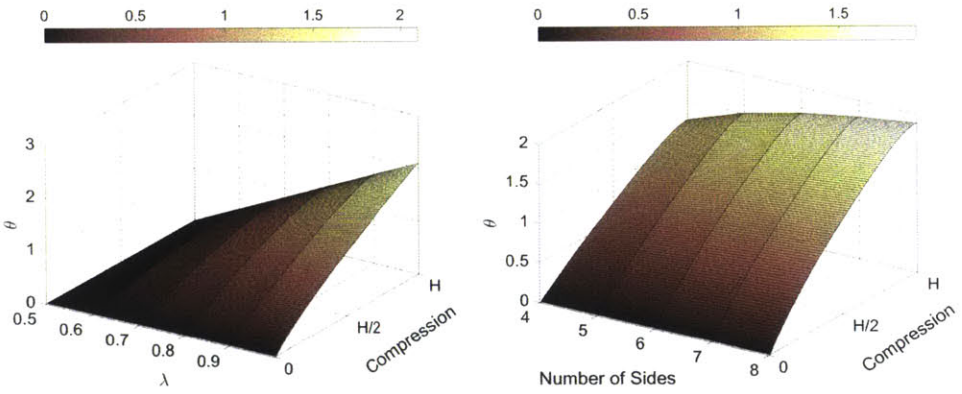

Figure 2-5: Rotation of the top surface (θ) with compression when $\lambda = 0.8$ and for $N = 5, 6, 7, 8$ and for $N = 6$ and λ varying between 0.4 and 1

From the previous section we have understood that the rotation of the top panel is necessary to maintain the prescribed kinematic and displacement boundary conditions while keeping the bottom fixed in a compression tension cycle of a Flexigami unit cell.

This provides us of another way to convert linear motion to rotary motion and vice versa which is generally achieved through rack-pinion assembly or through complicated process of carefully designing and machining CAMS. Flexigami towers are capable of generating complex profiles of linear-rotary motion conversion through their simple design and each curve is characterized by just three parameters N, λ and L. Figure. 2-5 represents selective few profiles of this conversion

THIS PAGE INTENTIONALLY LEFT BLANK

Chapter 3

Geometric Mechanics

The previous chapter detailed the important geometrical parameters which are necessary and sufficient to completely define a unit cell and delved deeply into the analysis of its geometry by understanding how each of the three defining parameters play a role in determining the shape, size and behavior of a unit cell. We discussed the kinematic coupling between the height of a tower and the rotation it induces in one of the two polygonal surfaces when the other is held fixed. We observed that the geometrical quantity γ exhibits a symmetric variation about half the maximum height (H) of a unit cell. This symmetric variation in γ is hypothesized to be one of the contribution factors why a *Flexigami* unit cell can exhibit snap through instability. To validate the predictions from kinematic analysis and to model the behavior of a unit cell in totality, we developed a numerical model of the unit cell. Here, we consider a unit cell with $N = 7, L = 30\text{mm}$ and λ is varied to span the entire range. All surfaces are assumed to be of uniform thickness t. Total energy of the system (E_T) is the sum of bending energy (E_B) of panels and energy stored in the creases (E_C)

$$E_T = E_B + E_C \tag{3.1}$$

Following sections details the procedure of computing these individual components

3.1 Bending of Triangular Panels

3.1.1 Isometric Deformations

The central problem in understanding the mechanics of a *Flexigami* tower is to find the equilibrium shape of the triangular panels as a function of the tower compression. Here we consider all the deformations of triangular panels to be isometric implying in-plane strains remain zero everywhere along the center surface. All isometric deformations can be characterized by a geometrical invariant of the surface called Gauss curvature. We need to incorporate equations of elasticity into the geometrical analysis to derive equations governing the deformations of the triangular panels under consideration.

In the Hookean elasticity, two dimensional strain along the center surface remains small, and the raii of curvature of the plate are much larger than the thickness, t. We keep the assumption of small displacement. Then the elastic energy per unit surface area stored in the plate is given by ([22])

$$\begin{aligned} E_{el} =& \frac{Et}{2(1-\nu^2)}\left[(\varepsilon_{xx}+\varepsilon_{yy})^2 - 2(1-\nu)(\varepsilon_{xx}\varepsilon_{yy}-\varepsilon_{xy}^2)\right]_{mid-plane} \\ &+ \frac{Et^3}{24(1-\nu^2)}\left[\left(\frac{\partial^2 w}{\partial x^2}+\frac{\partial^2 w}{\partial y^2}\right) - 2(1-\nu)\left(\frac{\partial^2 w}{\partial x^2}\frac{\partial^2 w}{\partial y^2} - \left(\frac{\partial^2 w}{\partial x \partial y}\right)\right)\right] \end{aligned} \tag{3.2}$$

where

- E - Young's modulus
- t - Material thickness
- ν - Poisson's ratio
- w - Out of plane deformations in the triangular panels

Isometric deformation of triangular panels have two parts to the calculation of the stored elastic energy, where

$$\text{Stretching Energy} : E_S = \frac{Et}{2(1-\nu^2)}\left[(\varepsilon_{xx}+\varepsilon_{yy})^2 - 2(1-\nu)(\varepsilon_{xx}\varepsilon_{yy}-\varepsilon_{xy}^2)\right]_{mid-plane} \tag{3.3}$$

$$\text{Bending Energy} : E_B = \frac{Et^3}{24(1-\nu^2)}\left[\left(\frac{\partial^2 w}{\partial x^2}+\frac{\partial^2 w}{\partial y^2}\right) - 2(1-\nu)\left(\frac{\partial^2 w}{\partial x^2}\frac{\partial^2 w}{\partial y^2} - \left(\frac{\partial^2 w}{\partial x \partial y}\right)\right)\right] \tag{3.4}$$

In the limit of isometric deformation, in-plane strain which is measured from the change in length of curves drawn along the center surface is zero. Hence, the elastic energy stored as stretching energy vanishes with this assumption. So, one hast o consider bending energy of the plates. The isometric deformations where all the surfaces are isometric to the plane are called develop-able surfaces. In these kind of deformations

$$\varepsilon_{xx}(x,y) = \varepsilon_{xy}(x,y) = \varepsilon_{yy}(x,y) = 0 \tag{3.5}$$

Hence, the contribution of stretching energy to the isometric deformations of triagular panels is zero. By minimizing the bending energies of these panels, one can derive the equilibrium shape of the tower in a compression cycle.

3.1.2 Computing Bending Energy

Energy stored in the triangular panels as they bend in the process of tower compression constitute the bending energy component of E_T.

Let the instantaneous height of the tower in a compression cycle be denoted by h. Each side of a tower consists of two triangular panels and three creases as shown in Figure 3-1. Co-ordinates of the points defining these two triangular panels are given by

- Point A: $[A_x, A_y, A_z]$; Point B: $[B_x, B_y, B_z]$;
- Point A' : $\left[A'_x, A'_y, A'_z\right]$; Point B' : $\left[B'_x, B'_y, B'_z\right]$

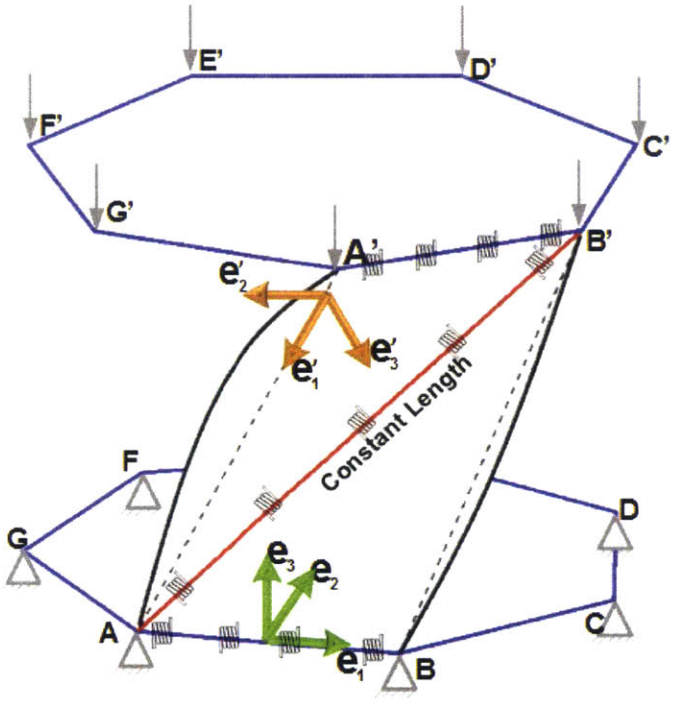

Figure 3-1: **Displacement and traction boundary conditions on Flexigami tower.** Bottom plate of the tower fixed in all six degrees of motion. Top plate is allowed to rotate about and have displacements along $\mathbf{e}_3$. Length of the diagonal crease AB′ is kep constant while the free edges AA′ are allowed to deform whose space curvature is determined. Diagonal valley folds, top and bottom mountain folds are modeled as torsional springs. Vertical displacement is applied on the model and total energy of the system is minimized.

Space curve $\mathbf{R}_{AA'}(s)$ is parameterized by the arc length s:

$$\mathbf{R}_{AA'}(s) = \left[|\overrightarrow{AA'}|s,\ \sum_{n=1}^{3} a_n \sin(n\pi s),\ 0 \right] \tag{3.6}$$

in the co-ordinate system of $(\vec{e_1'}, \vec{e_2'}, \vec{e_3'})$. By co-ordinate transformation, representation of $\mathbf{R}_{AA'}(s)$ in the co-ordinate system of $(\vec{e_1}, \vec{e_2}, \vec{e_3})$ is:

$$\begin{aligned} \mathbf{R}_{FE} &= \begin{bmatrix} Q_{11} & Q_{12} & Q_{13} \\ Q_{21} & Q_{22} & Q_{23} \\ Q_{31} & Q_{32} & Q_{33} \end{bmatrix} \begin{Bmatrix} |\overrightarrow{AA'}|t \\ \lambda sin(n\pi t) \\ 0 \end{Bmatrix} + \begin{bmatrix} A'_x \\ A'_y \\ A'_z \end{bmatrix} \\ &= \begin{bmatrix} Q_{11}|\overrightarrow{AA'}|\ s + Q_{12}\sum_{n=1}^{3} a_n \sin(n\pi s) + A'_x \\ Q_{21}|\overrightarrow{AA'}|\ s + Q_{22}\sum_{n=1}^{3} a_n \sin(n\pi s) + A'_y \\ Q_{31}|\overrightarrow{AA'}|\ s + Q_{32}\sum_{n=1}^{3} a_n \sin(n\pi s) + A'_z \end{bmatrix} \end{aligned} \tag{3.7}$$

where the components of the transformation matrix Q are given by :

$$Q_{ij} = e_i \cdot e'_j$$

Similarly, space curve $\mathbf{R}_{AB'}$ in the co-ordinate system $(\vec{e_1}, \vec{e_2}, \vec{e_3})$ is given by:

$$\mathbf{R}_{AB'}(s) = \begin{bmatrix} B'_x + s(A_x - B'_x) \\ B'_y + s(A_y - B'_y) \\ B'_z + s(A_z - B'_z) \end{bmatrix} \tag{3.8}$$

Assuming isomeric deformations of the triangular panels, three dimensional surface profile of the triangular panels at any instantaneous height (h) of a tower becomes developable. This developable surface of the triangular panel $(AA'B')$ is represented as a ruling joining corresponding points on two space curves $\mathbf{R}_{AA'}(s)$ and $\mathbf{R}_{AB'}(s)$

and mathematically written as

$$\mathbf{R}_{AA'B'}(s,v) = (1-v)\mathbf{R}_{AA'}(s) + v\mathbf{R}_{AB'}(s) \tag{3.9}$$

Similarly, for the triangular panel formed by the three points $BB'A$, it can be parametrically written as

$$\mathbf{R}_{BB'A}(s,v) = (1-v)\mathbf{R}_{BB'}(s) + v\mathbf{R}_{AB'}(s) \tag{3.10}$$

For a surface to be developable, it must also satisfy the condition that

$$\left(g(s) \times \frac{\partial g(s)}{\partial s}\right) \cdot \mathbf{R}_{AA'}(s) = 0; \quad \text{where} \quad g(s) = \mathbf{R}_{AB'}(s) - \mathbf{R}_{AA'}(s) \tag{3.11}$$

In order to solve for the equilibrium shape of the panels, total energy of the system which is sum of bending energy of panels and energy stored in the creases should be minimized subjected to the above stated constraints. Since, the triangular panels are modeled as developable surfaces, their bending energy is proportional to the surface integral of mean curvature squared ([4],[15]). Each side of an N sided, unit cell consists of two triangular panels ($AA'B'$ and $BB'A$). So, the bending energy associated with a single side is :

$$\text{Bending Energy} = K_B \int\int \left[H^2_{AA'B'}(s,v) + H^2_{BB'A'}(s,v)\right] \; \mathrm{d}s \; \mathrm{d}v \tag{3.12}$$

where $H_{AA'B'}$ and $H_{BB'A'}$ represent the mean curvature of the two surfaces and K_B is the bending rigidity of panels which is a function of Young's modulus (E), Poisson's ratio (ν) and material thickness (t).

3.2 Folding of Triangular Panels

For each of the N sides, we have three creases. Two corresponding to mountain folds joining each of the triangular panels to either of the polygonal surfaces. One valley fold which is the diagonal crease joining triangular panels. We consider the creases to be linear elastic torsional springs ([13]) whose torsional stiffness is denoted by K_c and non-zero rest state (θ_0) corresponding to zero crease energy. This non-zero rest state is the state in which a unit cell is fully open. Instantaneous fold angle of the crease at a point (θ_h) is obtained from the normals drawn on the two surfaces joining at that point. Following equations explain the procedure

- Gradient of $\mathbf{R}_{AA'B'}$ with respect ot v is

$$(\mathbf{R}_{AA'B'})_v = -\mathbf{R}_{AA'}(s) + \mathbf{R}_{AB'}(s)$$

$$(\mathbf{R}_{AA'B'})_v(t,v) = -\begin{bmatrix} Q_{11}|\overrightarrow{AA'}|\ t + Q_{12}\sum_{n=1}^{3} a_n \sin(n\pi s) + A'_x \\ Q_{21}|\overrightarrow{AA'}|\ t + Q_{22}\sum_{n=1}^{3} a_n \sin(n\pi s) + A'_y \\ Q_{31}|\overrightarrow{AA'}|\ t + Q_{32}\sum_{n=1}^{3} a_n \sin(n\pi s) + A'_z \end{bmatrix} + \begin{bmatrix} B'_x + s(A_x - B'_x) \\ B'_y + s(A_y - B'_y) \\ B'_z + s(A_z - B'_z) \end{bmatrix} \tag{3.13}$$

- Gradient of $\mathbf{R}_{AA'B'}$ with respect ot s is

$$\mathbf{R}_s(s,v) = (1-v)\begin{bmatrix} Q_{11}|\overrightarrow{AA'}| + Q_{12}\sum_{n=1}^{3} n a_n \pi \cos(n\pi s) \\ Q_{21}|\overrightarrow{AA'}| + Q_{22}\sum_{n=1}^{3} n a_n \pi \cos(n\pi s) \\ Q_{31}|\overrightarrow{AA'}| + Q_{32}\sum_{n=1}^{3} n a_n \pi \cos(n\pi s) \end{bmatrix} + v\begin{bmatrix} A_x - B'_x \\ A_y - B'_y \\ A_z - B'_z \end{bmatrix} \tag{3.14}$$

- Equation of normal ($\mathbf{N}$) to the tangent plane at a point (s,v) on the surface ($\mathbf{R}_{AA'B'}$) is given by

$$\mathbf{N}_{AA'B'} = \frac{(\mathbf{R}_{AA'B'})_s \times (\mathbf{R}_{AA'B'})_t}{|(\mathbf{R}_{AA'B'})_s \times (\mathbf{R}_{AA'B'})_t|} \tag{3.15}$$

- Similarly, equation of the normal ($\mathbf{N}$) to the tangent plane at a point (s, v) on the surface ($\mathbf{R}_{BB'A}$) is:

$$\mathbf{N}_{BB'A} = \frac{(\mathbf{R}_{BB'A})_s \times (\mathbf{R}_{BB'A})_t}{|(\mathbf{R}_{BB'A})_s \times (\mathbf{R}_{AA'B'})_t|} \tag{3.16}$$

To compute crease energy of a crease, we need to track the change in the angle of the crease along its length and integrate it. Following equations give the instantaneous angle at each of the three creases and energy stored in them

- Energy stored in the crease $A'B'$ at height h

$$\text{CreaseEnergy}_{A'B'} = \frac{K_C}{2} \int_{A'}^{B'} \left[(\theta_{A'B'})_h(0, v) - (\theta_{A'B'})_0(0, v)\right]^2 \mathrm{d}v \tag{3.17}$$

where

$$(\theta_{A'B'})_h(0, v) = \text{acos}\left((\text{N}_{AA'B'})_h(0, v) \cdot \vec{\mathbf{e}}_3\right)$$

- Energy stored in the crease AB' at height h

$$\text{Crease Energy}_{AB'} = \frac{K_C}{2} \int_{A}^{B'} \left[(\theta_{AB'})_h(s, 1) - (\theta_{AB'})_0(s, 1)\right]^2 \mathrm{d}s \tag{3.18}$$

where

$$(\theta_{AB'})_h(t, 1) = \text{acos}\left((\mathbf{N}_{AA'B'})_h(s, 1) \cdot (\mathbf{N}_{BB'A})_h(s, 1)\right)$$

- Energy stored in the crease AB at height h

$$\text{CreaseEnergy}_{AB} = \frac{K_C}{2} \int_{A}^{B} \left[(\theta_{AB})_h(0, v) - (\theta_{AB})_0(0, v)\right]^2 \mathrm{d}v \tag{3.19}$$

where

$$(\theta_{AB})_h(0, v) = \text{acos}\left((\text{N}_{BB'A})_h(0, v) \cdot \vec{\mathbf{e}}_3\right)$$

$$\text{Crease Energy} = \text{CreaseEnergy}_{A'B'} + \text{Crease Energy}_{AB'} + \text{CreaseEnergy}_{AB} \tag{3.20}$$

$$
\begin{aligned}
E_C &= \frac{K_C}{2}\int_{A'}^{B'} \left[(\theta_{A'B'})_h(0,v) - (\theta_{A'B'})_0(0,v)\right]^2 \mathrm{d}v \\
&+ \frac{K_C}{2}\int_{A}^{B'} \left[(\theta_{AB'})_h(s,1) - (\theta_{AB'})_0(s,1)\right]^2 \mathrm{d}s \\
&+ \frac{K_C}{2}\int_{A}^{B} \left[(\theta_{AB})_h(0,v) - (\theta_{AB})_0(0,v)\right]^2 \mathrm{d}v
\end{aligned} \tag{3.21}
$$

Therefore, for an N sided tower, total energy of the system

$$
\begin{aligned}
E_T &= N\left[E_B + E_C\right] \\
E_T &= NK_B \int\int \left[H^2_{AA'B'}(s,v) + H^2_{BB'A'}(s,v)\right] \mathrm{d}s\ \mathrm{d}v \\
&+ N\,\frac{K_C}{2}\int_{A'}^{B'} \left[(\theta_{A'B'})_h(0,v) - (\theta_{A'B'})_0(0,v)\right]^2 \mathrm{d}v \\
&+ N\,\frac{K_C}{2}\int_{A}^{B'} \left[(\theta_{AB'})_h(s,1) - (\theta_{AB'})_0 st,1)\right]^2 \mathrm{d}s \\
&+ N\,\frac{K_C}{2}\int_{A}^{B} \left[(\theta_{AB})_h(0,v) - (\theta_{AB})_0(0,v)\right]^2 \mathrm{d}v
\end{aligned} \tag{3.22}
$$

3.3 Results and Discussion

By minimizing E_T subject to prescribed kinematic and displacement boundary conditions at every discretized height of the unit cell in a compression cycle, we solve for the three coefficients $[a_1, a_2, a_3]$. This provides us with the space curves $\mathbf{R}_{AA'}$ and $\mathbf{R}_{BB'}$ and thus with the equilibrium shape of the triangular panels $\mathbf{R}_{AA'B'}$ and $\mathbf{R}_{BB'A}$ respectively. Figure. 3-2 show these equilibrium shapes at five positions of h in a compression cycle of a unit cell with $N = 7, L = 30\text{mm}, \lambda = 0.8$.

Parametric analysis of K_b and K_c helps us understand their individual roles in shaping the energetics of the system. Here we see that for lower ratios of K_b/K_c, implying for higher crease stiffnesses, the energy is continuously increasing (Figure. 3-3) implying mono-stability of the system. But as we increase the ratio, there is a gradual development of energy barrier(Figure 3-3) giving rise to two stable equilibrium

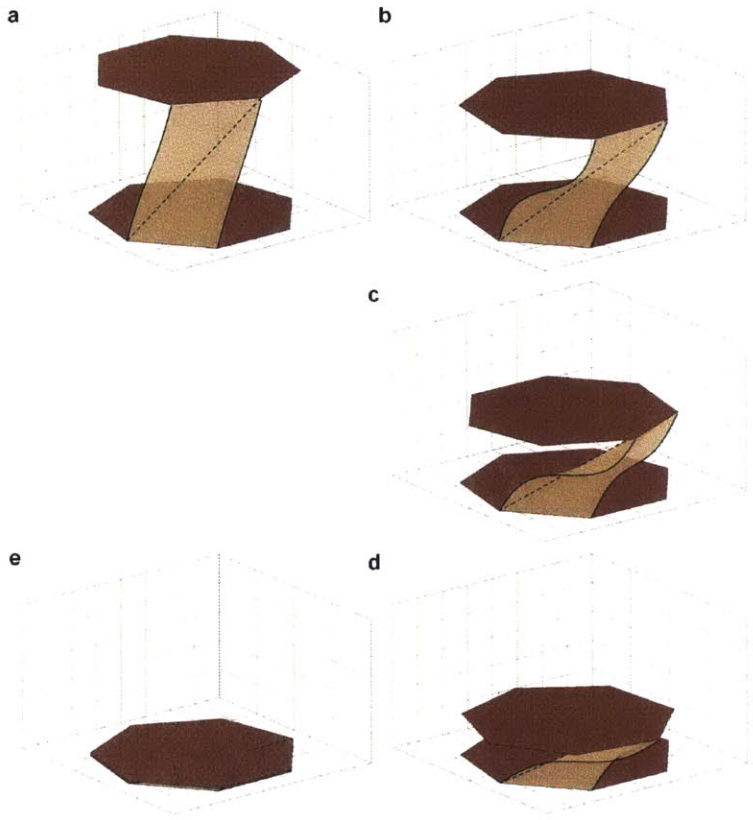

Figure 3-2: **Equilibrium shapes of the triangular panels in a compression cycle**. Total energy of the system E_T is minimized to obtain the three coefficients $[a_1, a_2, a_3]$ which define the equilibrium shape of the triangular panels. Figures a-e represent these equilibrium shapes in a compression cycle. Large out of plane deformations are observed as we see formation of clear S very similar to the profile observed in experiments.

positions and hence we can conclude that the system transitions from being mono-stable to bi-stable.

So, there is a critical ratio of K_b/K_c below which the system exhibits mono-stability and above which it exhibits bi-stability. This can be further intuitively understood by observing the individual energy profiles of bending energy and crease energy (Figure 3-4). Here we see that total bending energy has an energy barrier while total systems crease energy increases monotonically. Thus by finely tuning these individual bending and crease stiffnesses (K_b or K_c), response of a *flexigami* unit cell can be engineered to exhibit either mono-stability or bi-stability.

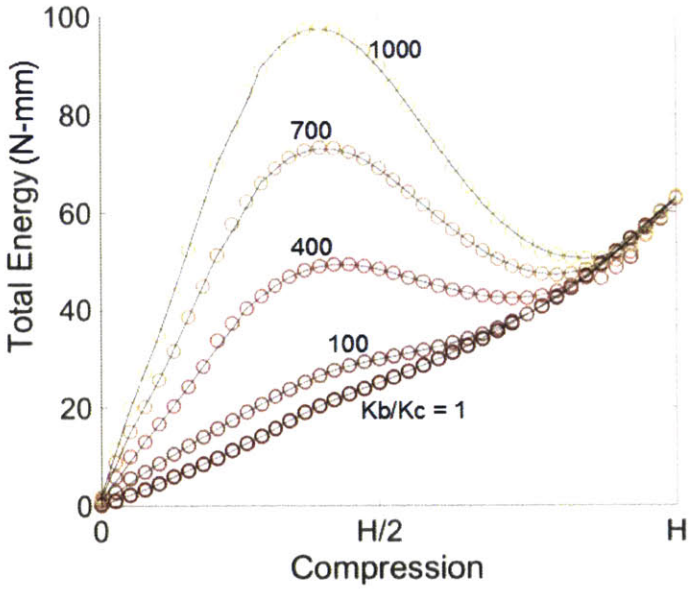

Figure 3-3: E_T: **Total Energy** Total energy of the system with two triangular panels and three hinges for different ratios of bending stiffness (K_b) and crease stiffness (K_c). For lower values of K_b/K_c, E_T exhibits monotonic increase representing monostability of the system. But as K_b/K_c increases, E_T develops an energy barrier which represents development of bi-stability in the system.

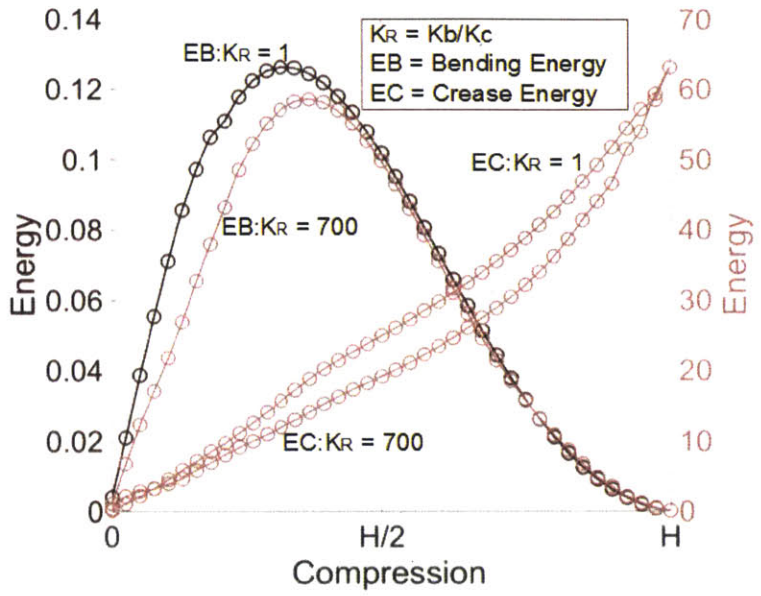

Figure 3-4: **Profiles of Bending energy (E_b) and crease energy (E_c) for two values of K_b/K_c.** For $K_b/K_c = 1$, we see that E_b is two orders of magnitude smaller than E_c. While E_b has an energy barrier about $H/2$, E_c is monotonically increases and E_T is dominated by E_c. But for $K_b/K_c = 700$, E_b and E_c are comparable and hence the total energy E_T exhibits a energy barrier representing bi-stability

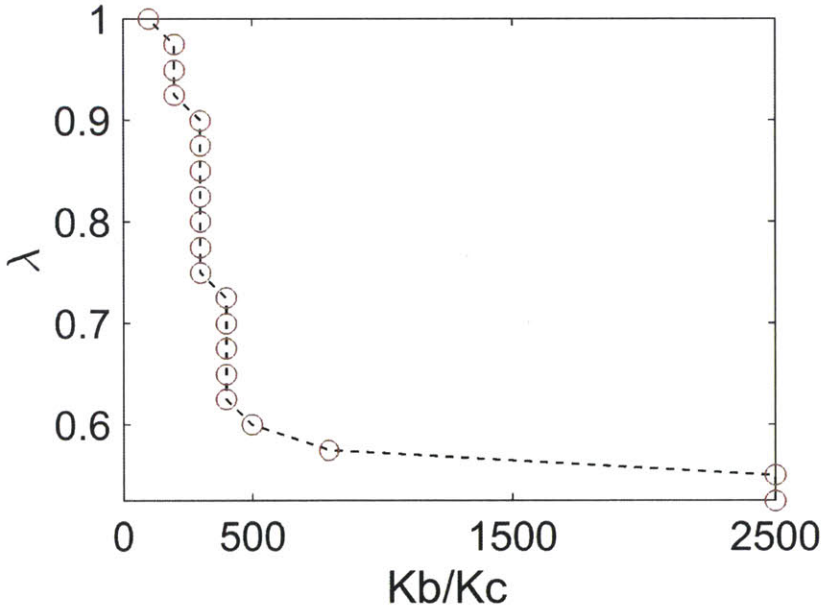

Figure 3-5: Phase diagram representing the transition between mono-stability to bi-stability as a function of Kb/Kc and λ for $N = 7$ and $L = 30$mm

Figure. 3-5 shows the phase diagram of the transition between the mono-stability and bi-stability for $N = 7,\ L = 30\text{mm}$ as we change λ and Kb/Kc.

3.4 Summary

Numerical model of a *Flexigami* unit cell provides us with the required understanding of the role of material properties in determining the behavior of a unit cell. Bending rigidity (K_B) of the triangular panels depend on the Young's modulus (E), Poisson's ratio (ν) and panel thickness (t). Creases which are modeled as torsional springs are governed by the torsional stiffness (K_C). Ratio of the stiffnesses of these two structural components of the tower ($K = K_B/K_C$) is an important quantity and also determines if a tower exhibits a bistable or monostable behavior. Total Energy (E_T) of the system which is the sum of bending (E_B) and crease (E_C) energies is dominated by E_C for higher values of K_C. Crease energy is always monotonically increasing and hence when E_C has major contribution towards E_T, we observe that the system exhibits mono-stability. But for higher values of K in which case bending energy provides major contribution to E_T, we have bi stability in the system.

THIS PAGE INTENTIONALLY LEFT BLANK

Chapter 4

Behavior of Flexigami Unit Cells under Compression and Tension

A *Flexigami* unit cells offers very interesting kinematic coupling between the extent through which it is compressed and the resulting rotation of one of the two polygonal surfaces while the other is held fixed. Rotation as well as simultaneous compression requires a custom made jig to hold the towers through a test. Here, in this chapter we detail the procedure of testing different kinds of sample unit cells fabricated from paper and understanding their force-displacement response when subjected to cyclic uni-axial compression tension tests in a displacement controlled environment

4.1 Experimental Design

4.1.1 Sample preparation

CAD models of 2D cut pattern of individual Flexigami unit cells are prepared and 120 watt Epilog mini laser cutter is used to cut a sheet of Daler-Rowney canford papers(150gsm or 90lb) into desired previously prepared 2D pattern. Figure. 4-1 represents the 2D cut pattern of a seven sided *Flexigami* cell. Here lines are represented using two colors. Black lines represent the outer boundary of the pattern and are cut at 75% speed, 60% power and frequency of 120Hz. While blue and red lines represent

creases and are formed by perforating the material along the lines at 80% speed, 2% power of the Epilog laser cutter and at 20Hz frequency. Once the sheet is cut into desired pattern, it is then folded sequentially along the creases with blue lines forming mountain folds and red lines forming valley folds. Tabs on the triangular panels are glued to the polygonal surface to obtain a closed volume of single Flexigami unit cell.

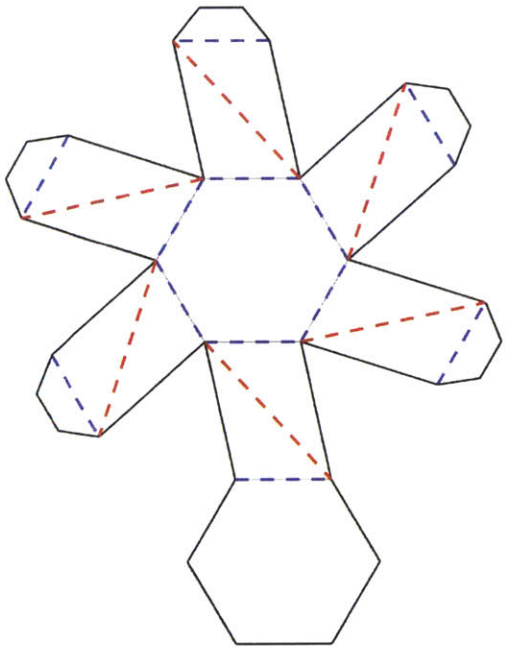

Figure 4-1: This figure represents the crease pattern along which the perforations are made using the epilog mini desktop laser cutter

4.1.2 Testing Apparatus and Procedure

A tensile testing machine (Zwick) is used to perform uniaxial tension-compression tests. As described in previous chapters, compression or tension of a *Flexigami* unit cell holding one polygonal surface fixed results in the rotation of the other polygonal surface. In order to obtain the true response of a tower under cyclic tension-compression environment, it is important that the experimental set up allows for

the free rotation of one of the two polygonal surfaces while holding the other fixed. To achieve this, we designed special jigs that can be attached to the Zwick testing machine.

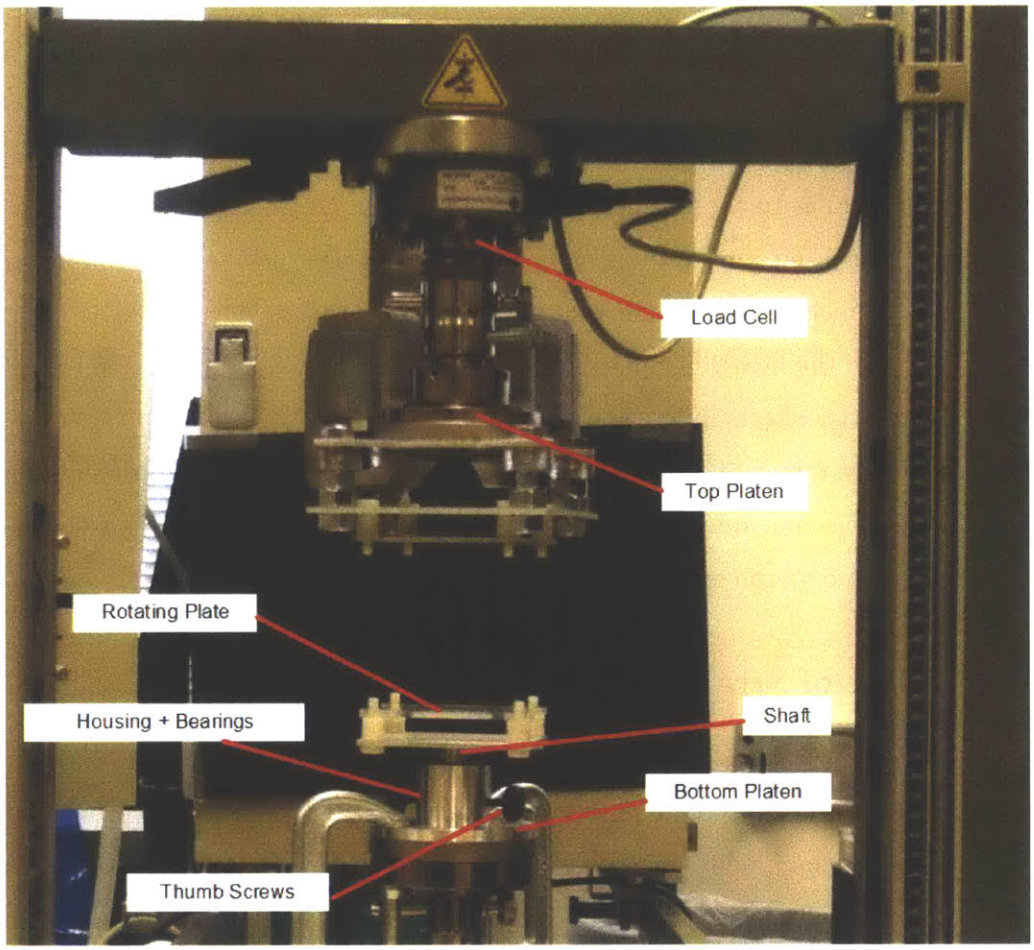

Figure 4-2: **Zwick mechanical testing machine**: This figure represents the mechanical testing machine used in this study. Load cell is in series to the grips which are labeled as top and bottom platens. Custom machined jigs to hold the tower in place are clamped to the machine grips in series. Tightening the thumb screws allows us to dynamically restrict the motion of the rotating plate.

Figure. 4-2 shows the specially designed jig which consists of double row angular contact ball bearing and a shaft whose end is press fitted into a plate to which towers are attached.The process of compression and tension tests on a tower in a cyclic fashion results in off centered loads on the shaft attached to the bottom plate.

These kinds of loads results in the swigging of the shaft when regular single row ball bearings are used. To avoid this, we used angular contact ball bearings which are well designed to bear off-centered loads on the shafts and still not introduce any slack into the system.

Figure. 4-2 shows the set up where the tower is fixed to the top and bottom plates using four nylon nuts and bolts. While the top plate does not allow for any rotation, bottom plate can be tuned to either allow free rotation or to not have rotation and effectively act similar to the top plate

Before carrying out any tests using mechanical testing machines, it is important to calibrate the machines and understand their hysteresis behavior as well as inertia effects because of the heavy jigs being used to hold the samples in place. We want to deal with these two effects independently.

To completely remove the hysteresis of experimental jigs and purely understand the hysteresis of the machine as well as intrinsic hysteresis of the structure we designed the following two experiments.

4.1.3 Effect of Strain rate

Here, we prepare two Flexigami cells whose geometry is defined by the following three parameters : $N = 4$, $L = 60$mm and $\lambda = 0.9$. We fold these two towers to result in opposite chirality and glue them back to back resulting in two layer Flexigami cells.

Now, this stacked Flexigami tower is secured to the top and bottom platens of the machine. Rotation of the bottom platen is restricted by tightening the thumb-screws (Figure. 4-2). Now, the towers are subjected to multiple cycles of compression and tension. These experiments are carried out in displacement controlled fashion. Rate of compression is varied for each cycle from 10mm/min to 100mm/min. Force displacement response of this tower structure under these varied strain rates is reported in Figure. 4-3.

Here we see that the compression or strain rate has very minimal effect on the peak force and all the force-displacement responses form a very nice tight band. But in the second half of the cyclic test when the tower is under tension we see that the

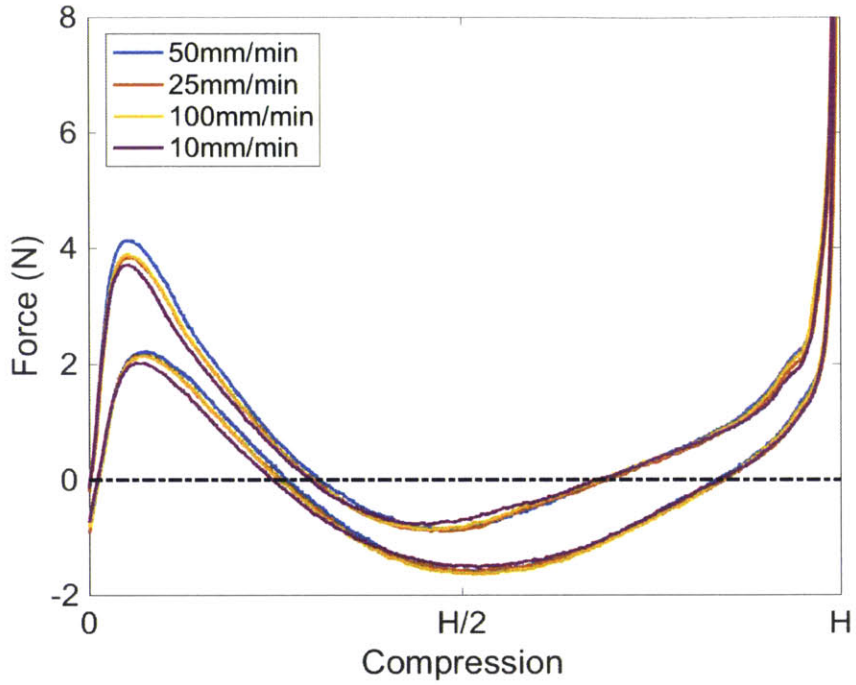

Figure 4-3: **Effect of strain rate on the response of flexigami towers**: Force displacement response of two layer flexigami tower of opposite chirality when the restriction of both the top and bottom platens are restricted to rotate and subjected to uni-axial compression tension tests under varied strain rates going from 10mm/min to 100mm/min. All the curves are overlapped on each other and they form a very tight band.

force response is deviated from the response of the compression cycle and exhibits large hysteresis and the observed hysteresis is independent of the strain rate.

In the next set of experiments we understand the inertial effects of the experimental jigs and their contribution to the force-displacement responses of the tower.

4.1.4 Inertial Effects of Customized Jigs

The jigs that are used to hold the towers in place are two orders of magnitude heavier than the test samples itself and the bottom rotating plate is an order of magnitude heavier than the test samples. If the bottom plate rotates in accordance with the kinematic constraints of the tower compression behavior, we need to understand the in detail how this effects the response recorded by the load cell which is in series with

the towers and the jigs.

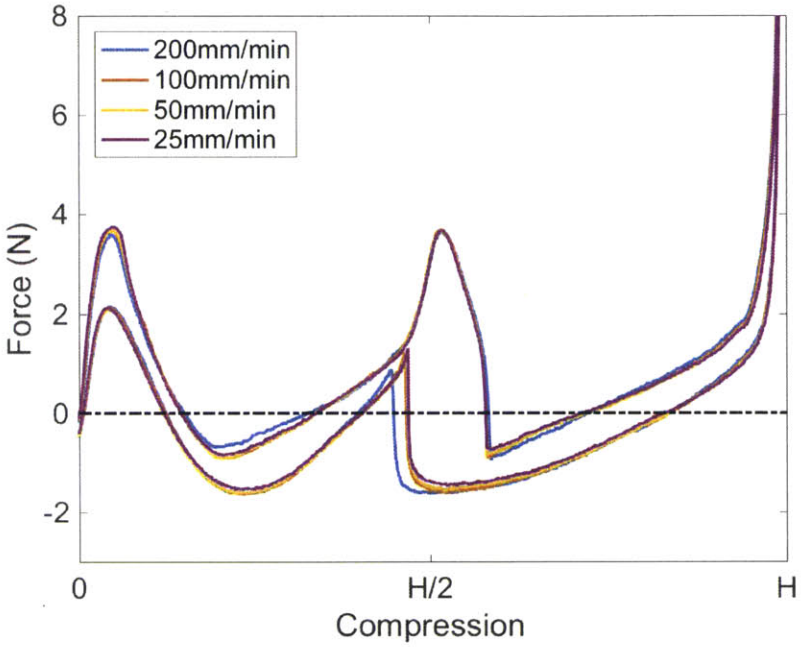

Figure 4-4: **Inertial effect of custom made jigs on the response of Flexigami towers-Exp1**: Force-displacement response of two layer Flexigami towers of opposite chirality when rotation of bottom platen is allowed and subjected to uni-axial compression tension tests under varied strain rates. All the curves are overlapped and it is observed that they form a tight band and have good agreement among them.

To capture this effect, we modified the boundary conditions of the previous experiment and now we allow for the rotation of the bottom platen while still restricting the rotation of the top platen. We now subject the tower to multiple cycles of compression and tension with different strain rates. Figure. 4-4 reports the force displacement response of the tower.

Here we observe that again all the response neatly overlap on each other forming a very tight band and the hysteresis is till large. To further confirm that the inertial effects are negligible at the current operating strain rates, we now carry out experiments on single layer towers having the same geometrical construction of $N = 4$, $L = 60\text{mm}$ and $\lambda = 0.9$.

This result gives the second confirmation that the effect of jig inertia on the force-

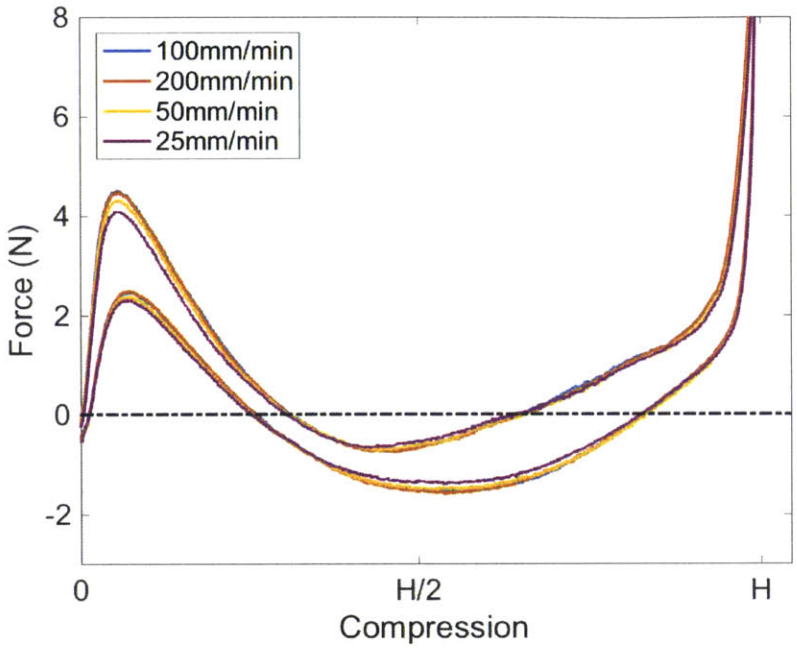

Figure 4-5: **Inertial effect of custom made jigs on the response of Flexigami towers-Exp-2**: Force-displacement response of single layer flexigami towers with rotation of the bottom plate allowed and subjected to uni-axial compression tension tests under varied strain rates. All the curves are overlapped and they form a tight band providing good agreement of response for varied strain rates.

displacement response of the towers is negligible at the current operating speeds. We recurrently observe huge hysteresis in the towers, independent of the strain rate or the rotation of the bottom platen. This strongly suggests that the observed hysteresis is intrinsic to the tower structure is not a contribution from the machine's hysteresis.

4.1.5 Hysteresis of the tower

Till now we have understood the inertial effects of jigs and strain rate on the force-displacement response of towers. In all these calibration tests, we have one recurrent phenomenon of large hysteresis. We hypothesized that the hysteresis is an intrinsic property of the tower and one of the contributing factors is the inter-panel contact which taken into effect beyond compression of $H/2$. To confirm this hypothesis we need to avoid this inter-panel contact and carefully observe the response of the tower.

The only way to achieve this is to sequentially remove the towers till we reach the situation where there is no panel-panel interaction. So, we first subject a single layer

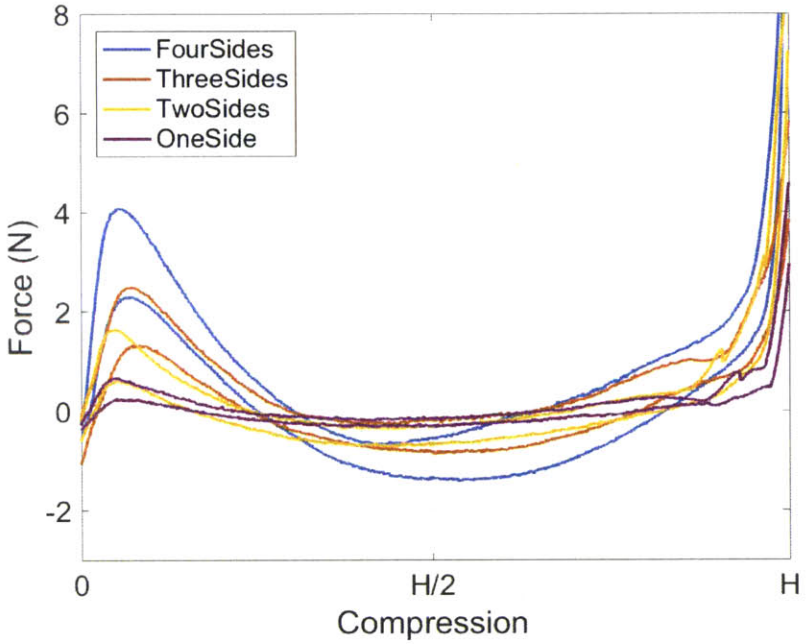

Figure 4-6: **Understanding hysteresis of the tower:** Force-displacement responses of single layer Flexigami tower subjected to uni-axial compression tension tests at strain rate of 25mm/min and allowing the rotation of bottom platen. Sides of the Flexigami tower are sequentially removed and the test is repeated. With decreasing number of sides, we observe reduction in the observed peak force and also the amount of hysteresis in a cyclic test confirming the role of panel-panel interaction to be the cause of hysteresis

tower with geometrical properties of $N = 4$, $L = 60$mm and $\lambda = 0.9$ and with all the panels in-tact to a compression tension cycle at 25mm/min . Next we remove one of the sides and repeat the experiment. Next we remove alternate side, so we have no panel-panel interaction and then finally we remove all the sides except one and repeat the experiment.

Figure. 4-6 reports these results. We see that as the number of sides reduces, the amount of hysteresis is also reduced and finally when we have just one side remaining, we observe that the hysteresis is at its minimum. From this result we can affirmatively state that the hysteresis is intrinsic property of the tower.

4.2 Results and Discussion

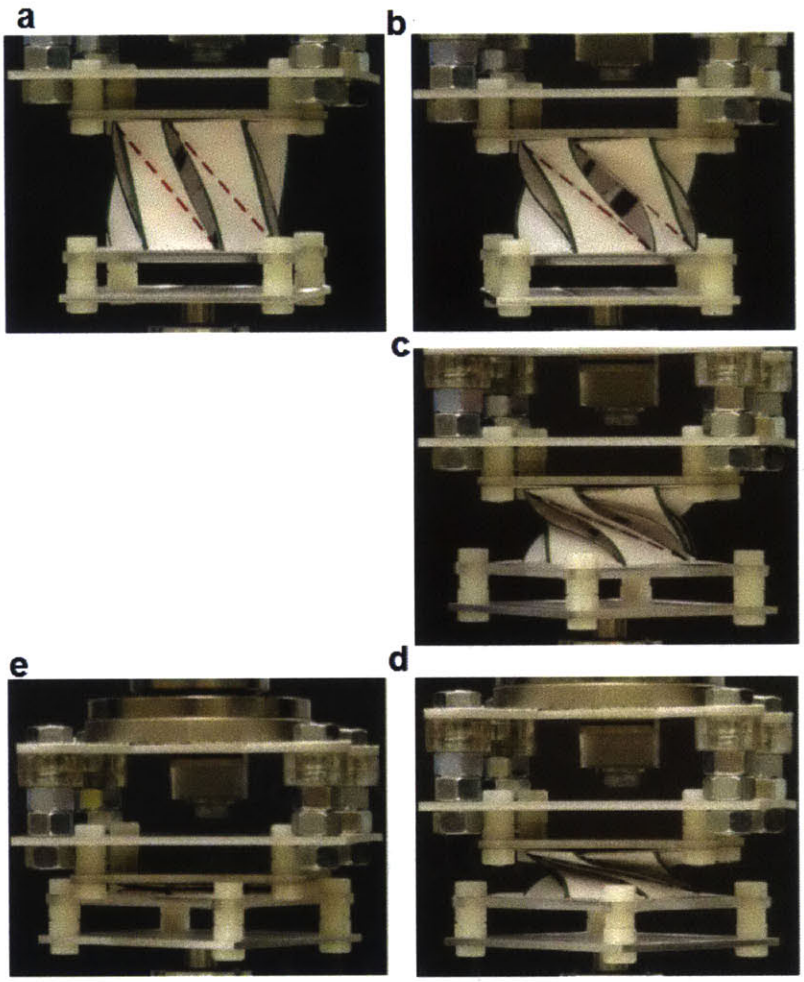

Figure 4-7: **Compression cycle of a flexigami unit cell**: This represents a compression cycle of a seven sided flexigami cell. Edges are marked green and the diagonal crease is marked red. We clearly observe the development and die down of an S shape as the tower is compressed. The diagonal crease marked red remains straight through out the compression cycle.

For $\lambda < \lambda_c$ the cell opens and closes smoothly; upon compression, the force increases gradually past relative displacement of $H/2$ and stiffens sharply only when the folded panels contact one another. For $\lambda > \lambda_c$, the cell exhibits a snap-through behavior where it jumps from one stable equilibrium position to another. In this case, the force first increases linearly until reaching a peak value (Figure. 4-8); at the

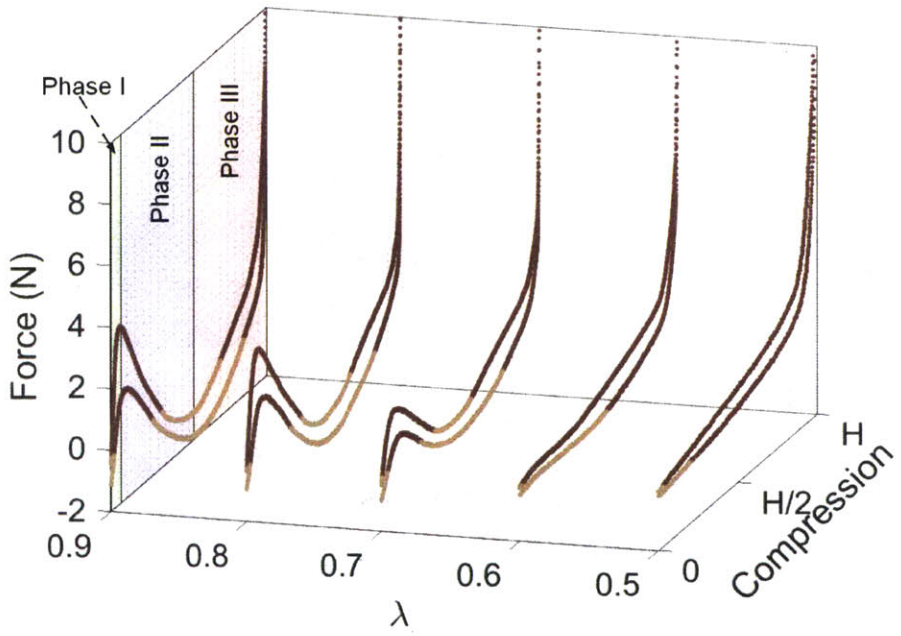

Figure 4-8: **Force displacement response of $N = 7$, $L = 30$mm and λ is varied**: For lower values of λ we observe monotonic increase of the force as the tower is compressed. But as λ is increased force barrier is developed which implies bi-stable nature of the system and strength of the bi-stability increases with increasing λ

instant of the peak force (F_P), the cell snaps causing a negative slope in the force-displacement curve. The force drops to a local minimum value, and then the cell strengthens with continued compression. Figure 4-8 pictorially represents the process of cell compression in a displacement controlled fashion. Here we clearly observe the development of out-of plane deformations which take the form of a skewed S shape in the initial stages of compression. These deformations become more pronounced resulting in peak force and start to die down in phase II (blue) of the force response cycle where we see a decrease in the force with increasing compression. Negative values of the force confirms the bi-stable nature of the unit cells which is absent when $\lambda < \lambda_c$. Once the adjacent panels comes into contact, the we enter phase III (red), where we observe strengthening of the force and its drastic shoot up as it is completely compressed.

Next, we see the variation in the responses when λ and L are kept constant while changing N. Figure. 4-9 represents this variation.

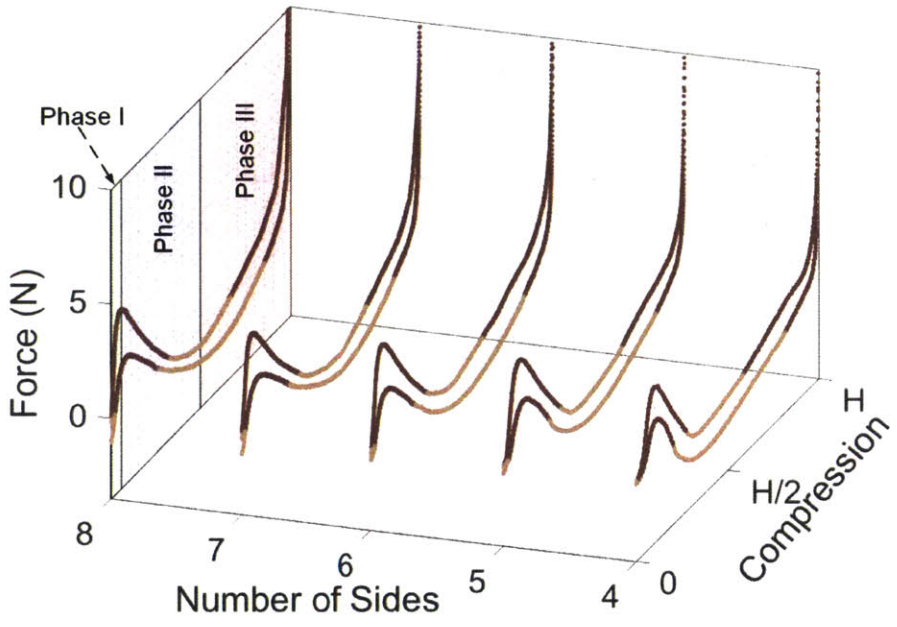

Figure 4-9: **Force displacement response of flexigami towers with** $\lambda = 0.9$ **and** $L = 30$mm **and** N **is varied**: Strong bi-stable nature is observed for all values of N and value of the peak force is comparable.

Important property to be investigated or understood of for any unit cell of a cellular material is its stiffness and the maximum force it can withstand. Figure. 4-10 summarizes the peak force distribution of flexigami unit cells as a function of N and λ. Here we see that for any constant N, peak force increases with λ

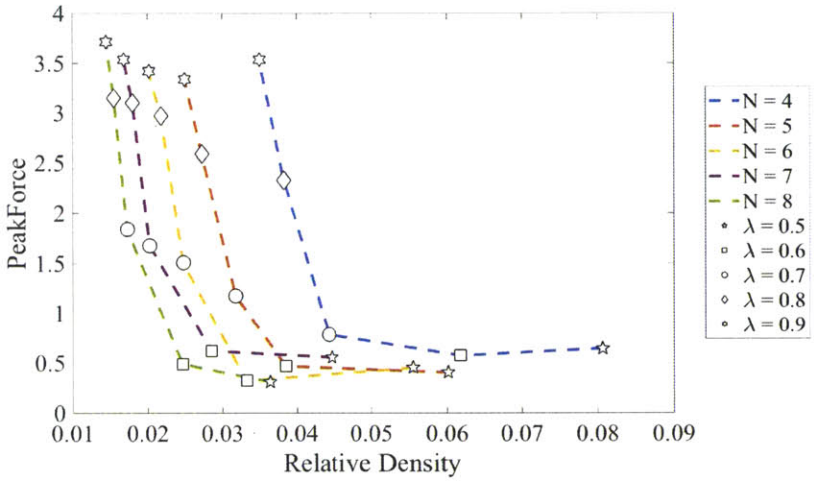

Figure 4-10: Peak force distribution of flexigami single layer towers as function of λ and N for $L = 30$mm

Figure. 4-11 reports the distribution of stiffness values for the same set of unit cells. Stiffness trend is similar to that of the peak force where we see decreasing value with λ for constant N, L. Compression at which peak force is attained for each of the bi-stable towers is very close. As stiffness is computed as ratio of peak force and the displacement (mm) at which this occurs, we see similar trend in both stiffness and peak force variations across all the cells with varying N and λ.

4.3 Summary

In this chapter we detailed the procedure of testing a *Flexigami* unit cell. Customized jigs are designed and fabricated to allow for smooth rotation as well as to be able to fix the bottom platen rigidly just by rotation of a thumb screw as the tower is subjected to cyclic uni-axial compression and tension tests. Top platen is always rigidly fixed independent of the boundary conditions offered by the bottom platen. Effect of the

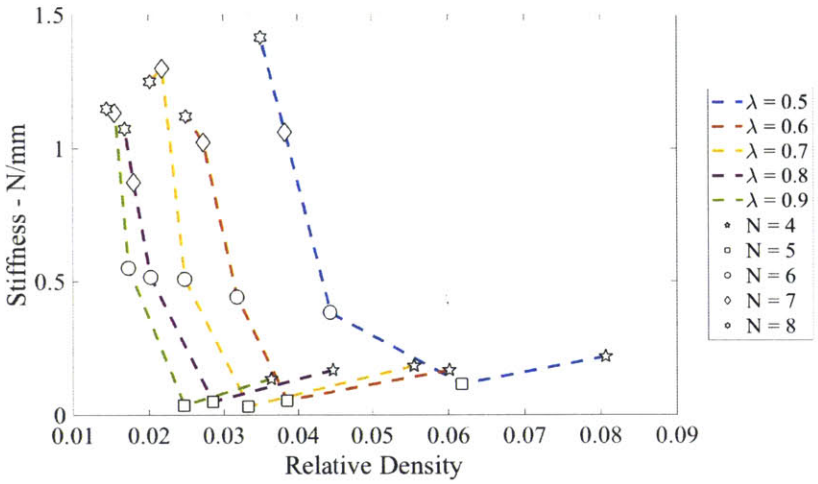

Figure 4-11: Stiffness distribution of flexigami single layer towers as function of λ and N for $L = 30$mm

compression and strain rate on the response of *Flexigami* cells is studied by subjecting a cell to cyclic compression tension tests under varied strain rates. It is concluded that the response of the tower is independent of the train rate in the measured range of values. Samples of unit cells with varying N and λ at $L = 30$mm are prepared and subjected to cyclic uni-axial compression tension tests. Observed peak force increases with λ when N and L are kept constant. This conclusion is in agreement with γ variations described in the Chapter 2. Peak forces and initial stiffnesses of unit cell matrix (Fig. 2-2) is summarized in Figures 4-10 and 4-11. Similar increasing trend of peak force as well as stiffness with λ is observed for all cases of constant N and L.

Chapter 5

Finite-element Analysis

Finite-element analysis is a great tool to simulate the behavior of Flexigami unit cells. It helps us look at individual contribution from each of the structural components to the overall behavior of the structure. The dynamic opening and closing exhibits snap through instability. To capture this unstable collapse, *Modified Riks Algorithm* is implemented ([1]). This algorithm is generally used to predict unstable, geometrically non-linear collapse of any structure. In this chapter we develop a finite-element model of *Flexigami* unit cell. For the sake of simplicity we modeled only one side of a seven sided cell. Each side consists of two triangular panels and three creases. Triangular panels are modeled with thin shell elements while creases are modeled as special torsional spring elements. Subsequent sections detail the procedure of developing and interpreting the results from FEM.

5.1 Material Characterization

5.1.1 Assumptions

Paper is generally considered to be orthotropic material. The thickness of the paper is much smaller compared to the other two in-plane directions. So, we can consider this as a case of plane stress. Under plane stress condition only the values of (E_1,E_2,ν_{12},G_{12},G_{13} and G_{23}) are required to define an orthotropic material. The

Poisson's ratio ν_{21} is implicitly given as $\nu_{21} = (E_2/E_1)\nu_{12}$. The stress-strain relations for the in-plane components of the stress and strain are of the form

$$\begin{Bmatrix} \varepsilon_1 \\ \varepsilon_2 \\ \gamma_{12} \end{Bmatrix} = \begin{bmatrix} 1/E_1 & -\nu_{12}/E_1 & 0 \\ -\nu_{12}/E_1 & 1/E_2 & 0 \\ 0 & 0 & 1/G_{12} \end{bmatrix} \begin{Bmatrix} \sigma_{11} \\ \sigma_{22} \\ \tau_{12} \end{Bmatrix} \tag{5.1}$$

To have a good estimate of the properties to be incorporated into the FE model, we need to characterize the paper being used in the experiments. For this we estimated the in-plane properties of the paper which is detailed in the following section.

5.1.2 Measurement of Mechanical Properties

It is very important to measure the properties of the paper that we are using as it significantly affects the experimental results and provides a realistic estimate for its in-plane properties. Here all through our experiments we use a single kind of paper canford (150 gsm). We need to determine its two in-plane modulus (E_1, E_2), Poisson's ration ν_{12} and the shear modulus G_{12}. ISO1924-2 standards are followed to carry out the required experiments

Papers are made from cellulose fiber and during the process of manufacturing, the axes of the fibers tend to be aligned parallel to the paper flow through the paper machine. This phenomenon leads to anisotropy in the mechanical properties of paper. Specimens conforming to ISO standards were cut in three different orientations as shown in Figure.5-1 using a desktop mini Epilog laser cutter. 10 samples are cut in each direction with the specified dimensions and are speckled with silver sharpie to be able to use Digital Image Correlation (DIC) technique for the estimation of in-plane strains.

5.1.3 Testing Apparatus and procedure

In order to determine the in plane modulus and Poisson's ratio, we should have information about strains developed in the specimen in the longitudinal and transverse

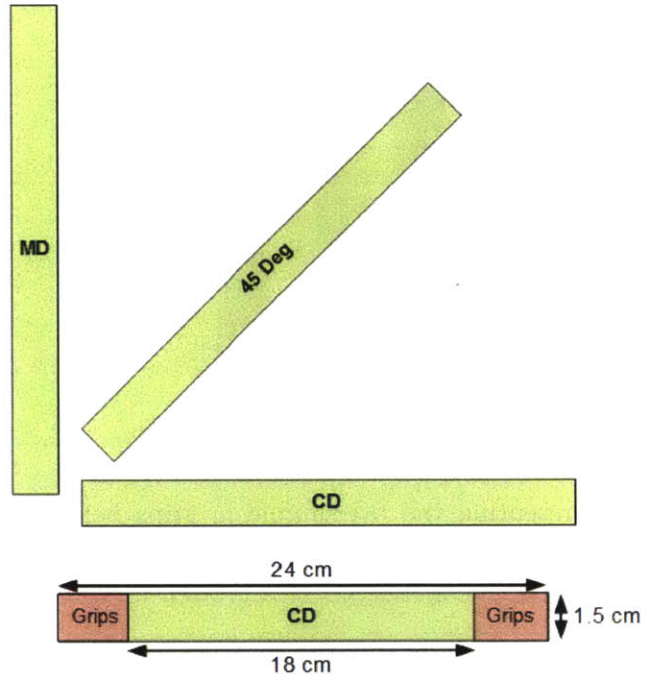

Figure 5-1: Representative figure of the directions along which the samples are cut from a Daler-Rowney Canford paper and the dimensions of the sample conforming to ISO standards for paper testing.

directions. Since, attaching a strain gauge would significantly affect the properties of paper and would result in only one data point, we used the Digital Image Correlation (DIC) which is a non-contact optical strain measurement technique. Tests were conducted under displacement controlled conditions where the specimen was pulled at a constant velocity of 20mm/min with a 10KN load cell. A series of images of the specimen being deformed are captured and analyzed with Vic-2D. This provides us with the data of in-plane strains. All the samples that break within 10mm of the clamping distance are rejected to meet with the ISO standards.

5.1.4 Results and Discussion

In-plane stress-strain curves of the Daler-Rowney canford (150gsm) paper are represented in figure. 5-2. Strong anisotropy of the paper is very clearly represented by these stress-strain profiles. While the modulus along the Machine Direction (MD) is

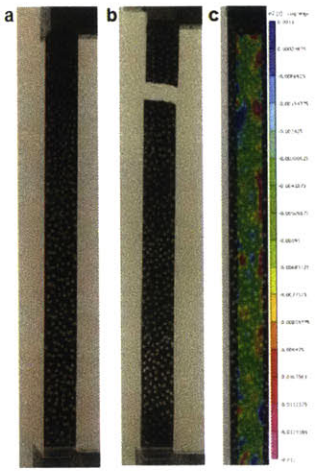

Figure 5-2: Figure representing the (a) sample in grips before the test (b) after breakage and (c) representative set of longitudinal strains developed at the maximum extension

the highest, modulus along the Cross Direction (CD) is the least.

	Modulus (GPa)
MD (E_1)	6.83
CD (E_2)	3.11
G_{12}	2.17
ν_{12}	0.23

Table 5.1: Mean values of the modulus and Poisson's ratio

Figure. 5-3 shows the stress-strain response of the paper sample in the three directions. We see that the material has highest toughness (area under stress-strain curve) in the Machine Direction and lowest in the Cross direction. Table 5.1 lists the average Young's modulus along the two major directions (Machine direction and Cross direction) as well as shear modulus (G_{12}) and measured Poisson's ration ν_{12}

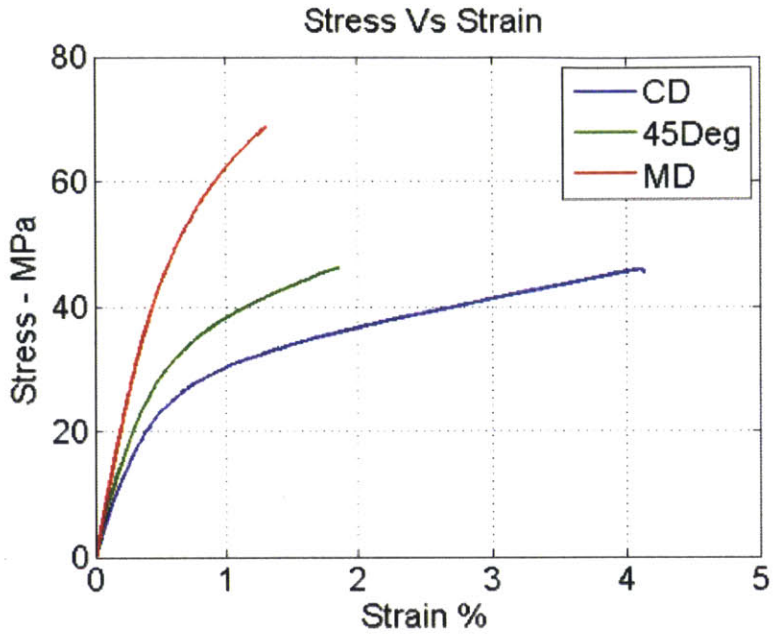

Figure 5-3: Stress-strain response of the paper strips in the three measured directions

5.2 Developing Finite-Element model

Since our primary objective is to understand the intricate details of the Flexigami tower snapping mechanism and to delineate the contributions from each of the structural components we developed a finite-element model of the tower with one side. Each side of a Flexigami tower is a combination of two triangular panels, one valley fold and two mountain folds. Triangular panels are modeled as thin shell structures whose behavior is defined by its shell thickness, Material density, and the six in-plane material properties as detailed below. These properties also determine the individual bending rigidity (K_b) of the triangular panels. Both mountain and valley folds are modeled as linear elastic torsional springs whose behavior is determined by the torsional spring constant (K_c). Element type of STRI3 in Abaqus/Standard is used are used to mesh the triangular panels along with top and bottom polygonal surfaces. The element has three nodes, each with six degrees of freedom. The strains are based on thin plate theory, using small-strain approximation. Total of 13,960 STRI3 elements are used to mesh top and bottom plates; while, 6568 STRI3 elements are

used to mesh each of the triangular panels. To model creases we use special purpose spring elements whose associated action is defined by the specified degrees of freedom involved. Type I and Type II creases are discretized into 9 and 17 points where these spring elements are acting.

Specimen is then subjected to vertical displacement while fixing bottom plane (Figure. 5-5s) and imposing penalty to avoid node penetration between the two triangular panels which would come in contact in the process of compression. External work done on the entire specimen and reaction forces at each and every node (from individual frames) on top and bottom panels of the specimen are obtained as output from the FE model. Vector summation of these reaction force components will result in the Force-Displacement curve.

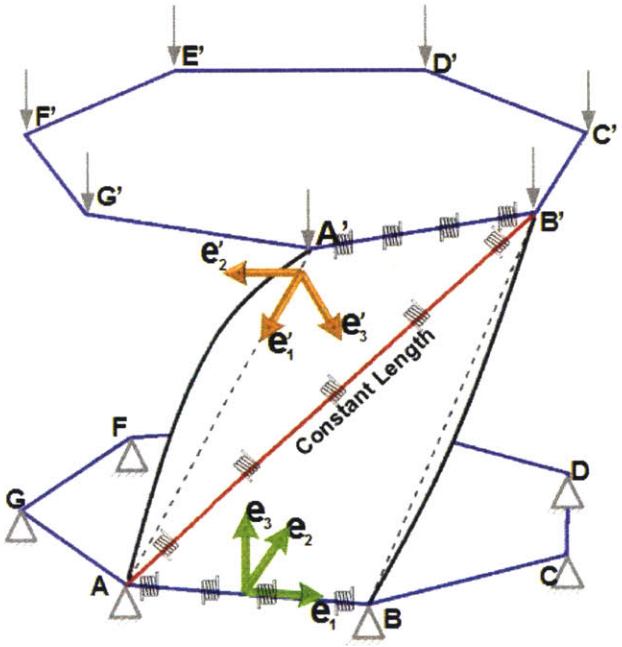

Figure 5-4: **Geometry of the model used in FE Simulations**

5.3 Results and Discussion

These simulations also allow us to extract reaction forces developed at each and every node of the top and bottom polygonal surfaces. Vectorial addition of these individ-

ual components over the entire mesh gives us instantaneous force and tracking this instantaneous force results in the force-displacement profile of a single compression cycle. Figure. 5-5 shows the process of a compression cycle and Mises stress developed in the cell. Stresses in the triangular panels are an order of magnitude smaller than stresses in the creases. We see stress concentrations mainly in the elements connected to the springs. Creases are the regions of high stresses and strains and play an important role in moment transfer between the panels. To compare the results of these

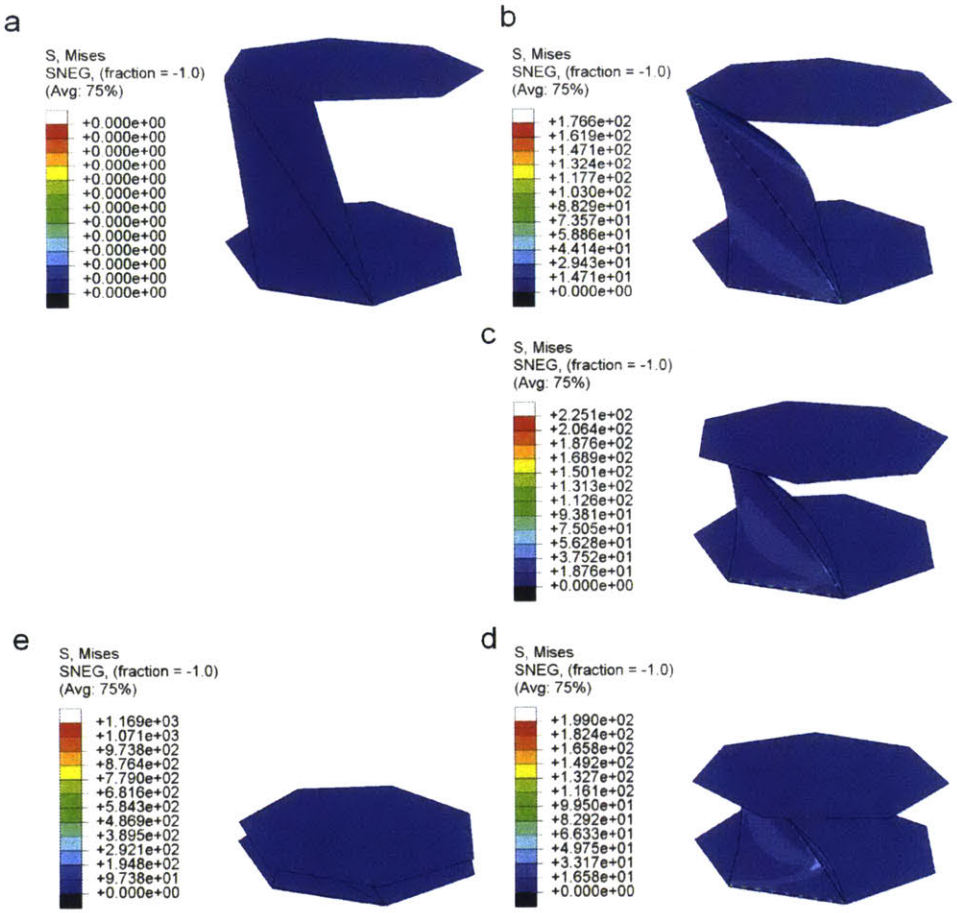

Figure 5-5: Mises stress in the cell in a compression cycle

simulations with experimental observations, we amplified the response by seven times and overlapped with the corresponding experimental results as shown in Figure 5-6. Here we are referring to the particular case of $N = 7, \lambda = 0.8$. We see that the ini-

tial stiffness of the system from finite-element simulations overshoots experimentally observed stiffness. We know that paper can be plastically deformed over repetitive cycles. The measured responses of the unit cells are from the samples that were previously subjected to cyclic compression and tension over repetitive cycles. This process reduces the stiffness of creases which in-turn affects the force-displacement behavior recorded during the experiments. But, the predicted negative force from FEM matches agreeably with the experimental results.

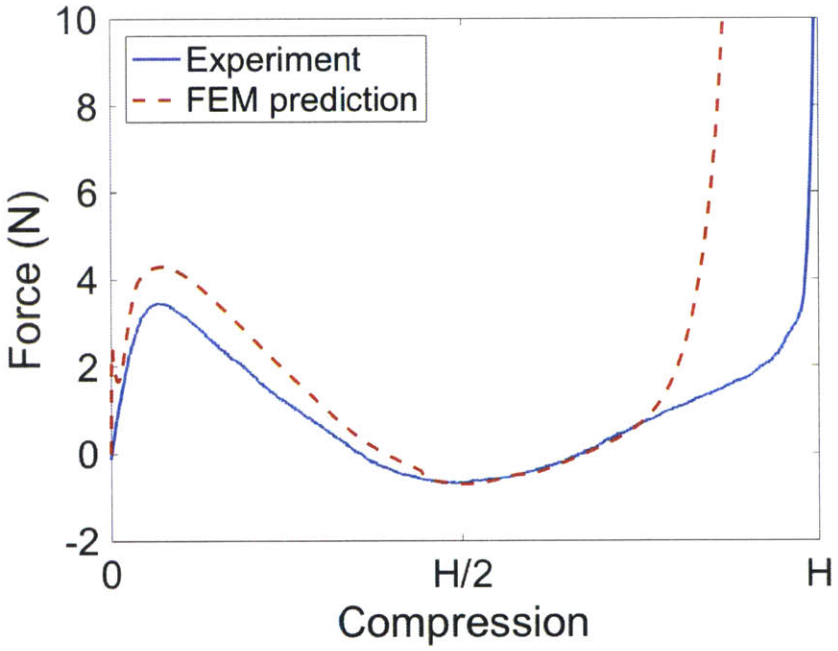

Figure 5-6: Force displacement response of a Flexigami tower in a compression cycle from FEM as compared to experimental results

5.4 Summary

Development of a finite-element model allows us to simulate the force-displacement behavior of a unit cell. To model the behavior accurately, good estimation of material properties is required. Hence, the paper which is used to fabricate the experimental samples is characterized. Required orthotropic properties are estimated. Stresses and

strains developed in each of the individual structural element can be easily visualized. From the model, we understood that very high stress concentrations are developed along the creases. Hence, yield strength of the material along the creases play an important role in maintaining the structural integrity of the system. It should be capable of withstanding high stresses over repeated cycles.

THIS PAGE INTENTIONALLY LEFT BLANK

Chapter 6

Stacked Flexigami cells and Mechanisms

6.1 Flexigami cells in series

In the previous chapters we explored the mechanics of single *Flexigami* unit cells and understood the role of individual structural components of the system in shaping its mechanical response.

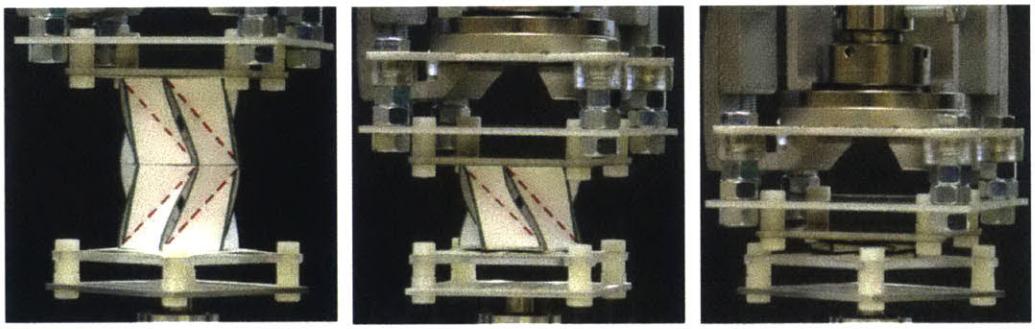

Figure 6-1: **Sequential compression of Flexigami cells**. This figure represents the response of two flexigami cells of opposite chirality glued back to back and subjected to uni-axial compression tests. Rotation of top platen is restricted while bottom platen is allowed to rotate resulting in sequential compression of the tower assembly.

Now, we will understand the effect of boundary conditions and how changes in them affects the response of tower assemblies. A simple assembly of Flexigami consists of two towers attached back to back as showin in Figure 6-1.

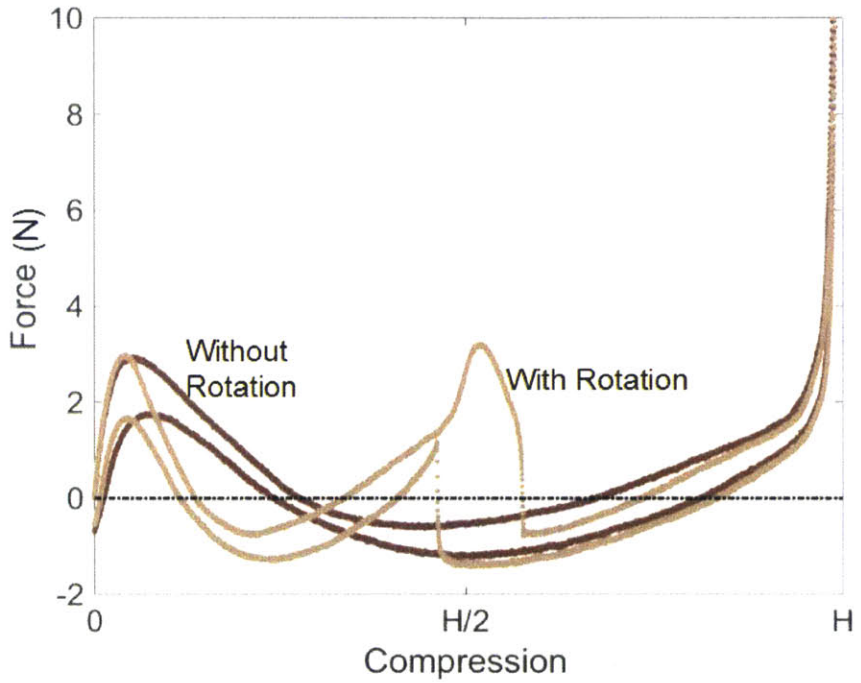

Figure 6-2: **Force displacement response of Flexigami cells in series under different displacement boundary conditions**.Configuration 1 represents the boundary condition in which rotation of top and bottom platen is restricted resulting in the simultaneous compression of both the towers resulting in a single peak. Configuration 2 represents the boundary condition in which rotation of the top platen is restricted while bottom platen is allowed to rotate resulting in sequential compression of the towers and thus having two peaks each corresponding to a tower in the series assembly.

Here we present the results when two towers with same geometrical parameters ($N = 7,\ L = 30\text{mm},\ \lambda = 0.8$) folded to result in opposite chirality are attached back to back. From previous discussion, we understand that as a result of *Flexigami*'s geometrical construction, compression of a unit cell while fixing one of the two polygonal surfaces results in the rotation of the other. In two cell assemblies we have three surfaces (one surface being common to both the towers when attached back to back). While the top surface is always fixed, we can choose to not fix the bottom surface

and thus we have two different boundary conditions under which this assembly can be compressed.

6.1.1 Two Layer Cellular Structure With Rotation

Here we allow the rotation of the bottom surface. So, when the two tower assembly is subjected to displacement controlled uni-axial compression, we observe sequential collapse (Figure 6-1)of each of the towers. When bottom tower is being compressed, middle surface remains stationary and results in the rotation of bottom platen. Once the bottom tower is completely collapsed, we see the compression of top tower. Bottom platen along with the compressed tower acts as a unit and rotates while the top tower is being compressed. Force displacement response (Figure 6-2)of this particular configuration has two peaks corresponding to each of the tower.

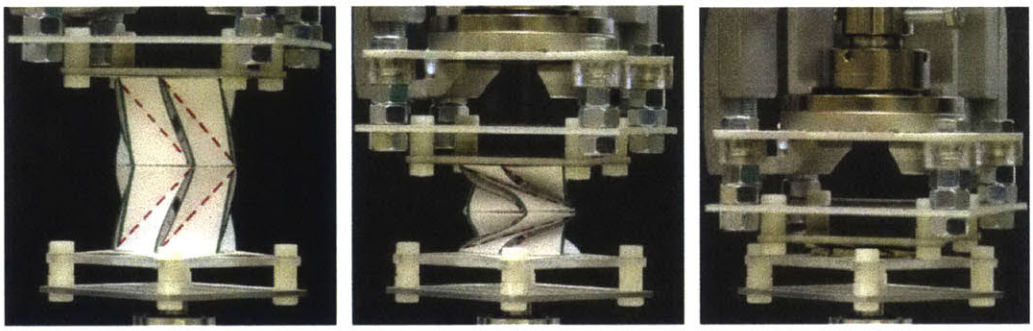

Figure 6-3: **Simultaneous compression of Flexigami Cells**. This figure represents the response of the two Flexigami cells of opposite chirality glued back to back and subjected to uniaxial compression tests. Rotation of top and bottom plates is restricted resulting in simultaneous compression of the tower. Middle plane is rotated in the process of compression making it possible for both towers to have simultaneous compression.

6.1.2 Two Layer Cellular Structure Without Rotation

Here, we restrict the rotation of both the top and bottom platens. Now, when the two tower assembly is subjected to the same displacement controlled uni-axial compres-

sion, we see that both the towers start to get compressed simultaneously (Figure 6-3) as opposed to sequential compression observed in the previous case. As both top and bottom plates are restricted to rotation, compression of either of the towers results in the rotation of the middle common surface which in turn results in the compression of the other tower and as a result we observe simultaneous compression. Force displacement response (Figure 6-2) of this configuration exhibits a single peak which is in agreement with the observed behavior.

These two force displacement responses of a single structure when subjected to different boundary conditions represent a strong case of *Flexigami*'s capability to tune its internal folding mechanisms to meet with different external boundary conditions with out catastrophic failure of the structure. This also opens the pathway to the idea of carefully engineering these configurations of cellular assemblies capable of reproducing any given curve as their force response when different boundary conditions are imposed.

6.1.3 Multi Layer Cellular Structure

More complex assemblies of unit cells are prepared by stacking unit cells of same $N = 7$, $L = 30$mm and $\lambda = 0.5, 0.6, 0.7, 0.8, 0.9$. Out of 3125 possible combinations of all these cells, we chose four representative combinations two of which are shown in Figure 6-5.

Again we subjected these four assemblies to displacement controlled uni-axial cyclic compression and tension tests. We observed that independent of the sequence in which these individual unit cells are arranged to form a particular combination of an assembly, their force displacement response is the same. They overlap on each other very neatly. This response (Figure. 6-4) is a resultant of their individual peak forces required to compress them.

In the previous sections we have seen that the peak force required to compress a unit cell increases with increasing λ for a constant N, L. So, when they are stacked in series to form one single assembly and subjected to displacement controlled compression, the unit cell which requires least amount of force gets compressed first

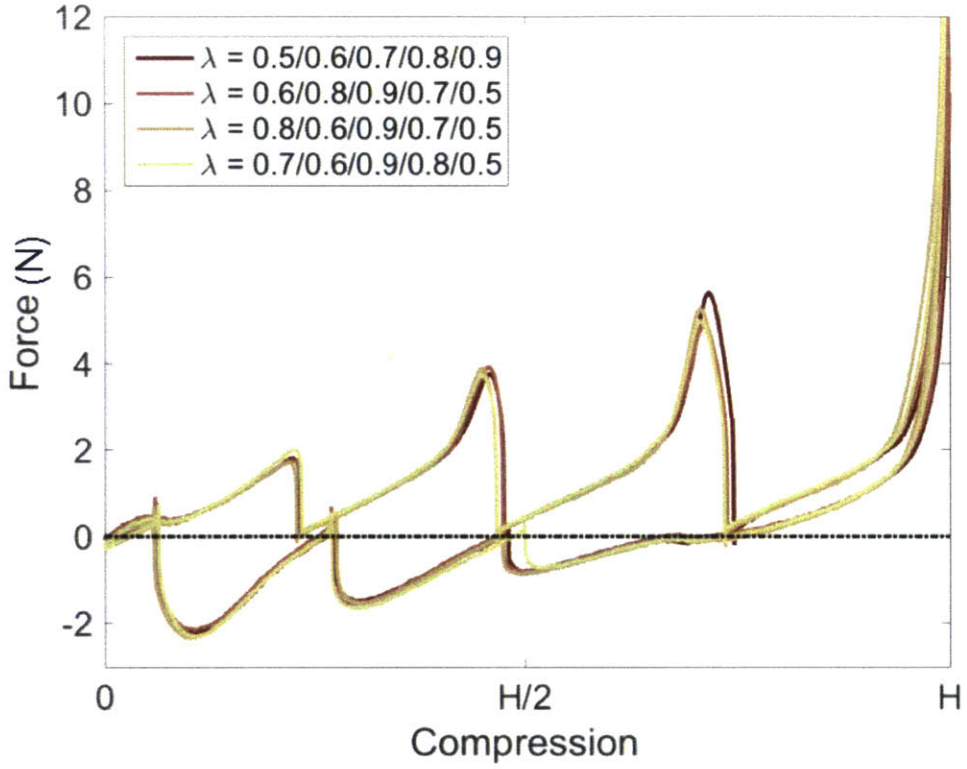

Figure 6-4: **Force displacement response of stacked Flexigami cells with varying** λ. This figure represents the force displacement response of four different configurations of Flexigami cells stacked in series with varying λ and subjected to uniaxial compression tension tests in a displacement controlled manner. All the responses form a very tight band and show good agreement with each other confirming that the softer tower gets compressed or opened up first irrespective of the configuration in which these unit cells are arranged

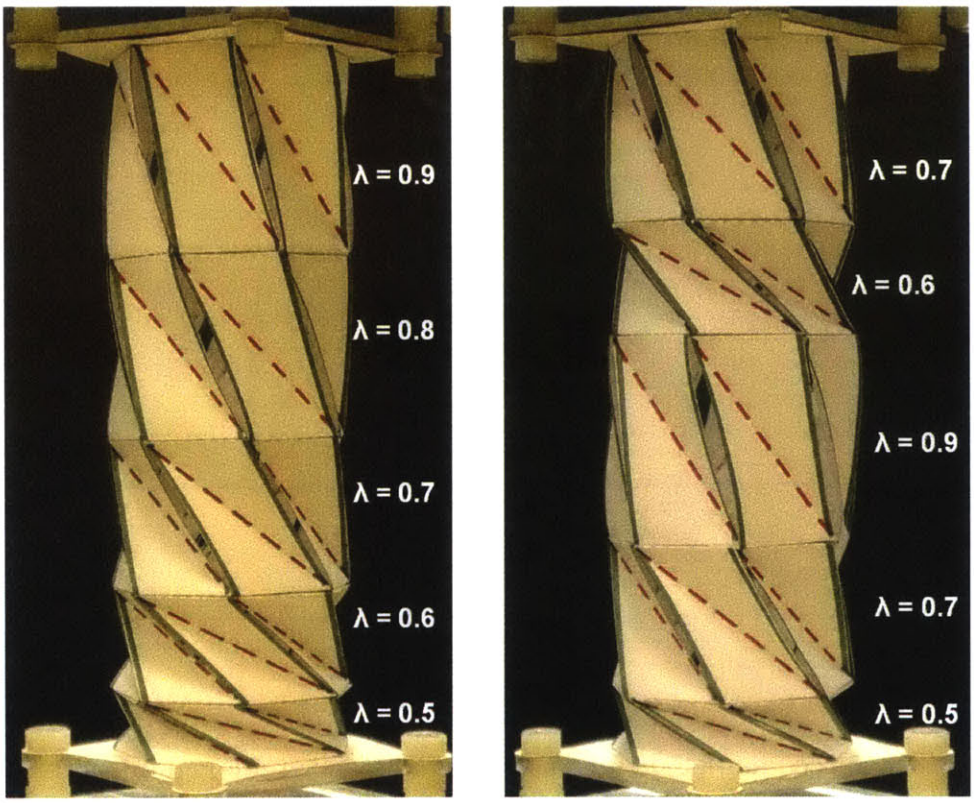

Figure 6-5: Flexigami cells stacked in series of constant $N = 7$ and $L = 30$mm but λ is varied from 0.5 to 0.9. Here we present two representative configurations from the total number of possible combinations.

and it will also be the first unit cell to open up in the tension. We also, observe that the minimum amount of force recorded by the tensile testing machine in compression only part of the cyclic test is zero but not negative which should correspond to the snapping of individual unit cells. A unit cell subjected to cyclic compression tries to resist the imposed compression resulting in the positive force recorded by the tensile testing machine, but once it is compressed beyond a threshold limit, it is has a greater tendency to move towards a completely closed state and hence it starts to exert a pulling force which is recorded as negative force response by the tensile testing machine. But, when these unit cells are stacked in series, we see that, while resistance of a unit cell in the assembly to get compressed is recorded as positive force response, its tendency to exert a pulling force which should be recorded as negative force response is missing and that this pulling force of the cell being compressed is compensated internally by immediate cells on either side.

6.2 Flexigami cells in parallel

This sections explores the properties of the *Flexigami* cells tiled in a plane. This behavior is similar to the behavior of springs in parallel. Here we present the results two stacked towers are placed in parallel and subjected to compressive forces individually and simultaneously.

Figure. 6-6 shows the response of the tower made from gluing two towers of opposite chirality back to back subjected to uni-axial compression test with out allowing the rotation of top and bottom platens. As discussed previously, this results in the simultaneous collapse of the both the towers resulting in single peak in its force displacement response.

In order to tile two towers in parallel, they should be having same free standing height in a completely stress free state. To achieve this, we halved the dimensions of the towers used in Figure 6-6 and now constructed a tower with four unit cell with alternating chirality. When this configuration is subjected to the similar uni-axial compression test conditions by restricting the rotation of both the platens, we

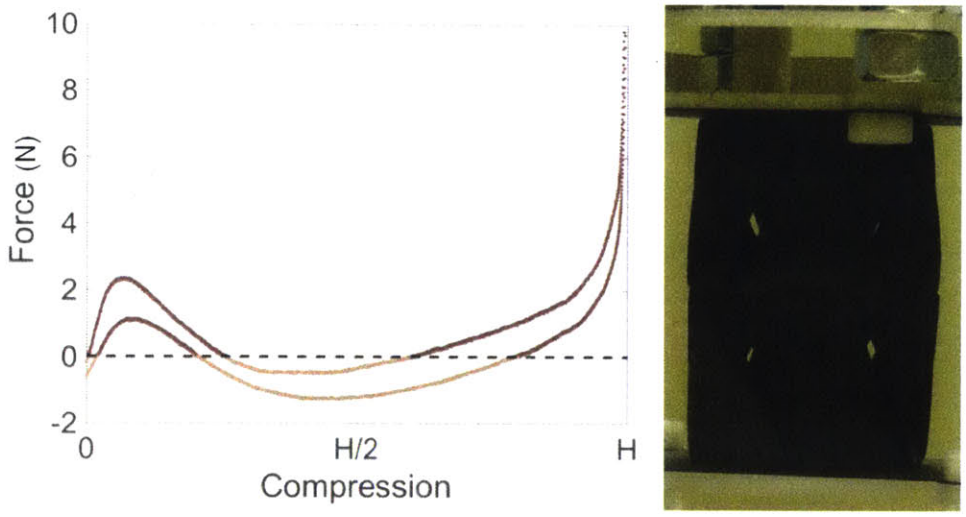

Figure 6-6: Force displacement response of two Flexigami cells when both the platens are restricted to rotate and subjected to uni-axial compression tension test

observe two peaks in its force displacement response as opposed to one peak that is previously observed. This is the resultant of simultaneous compression of the towers in two stages. Top and the bottom most towers are compressed initially followed by the compression of the two towers in the center.

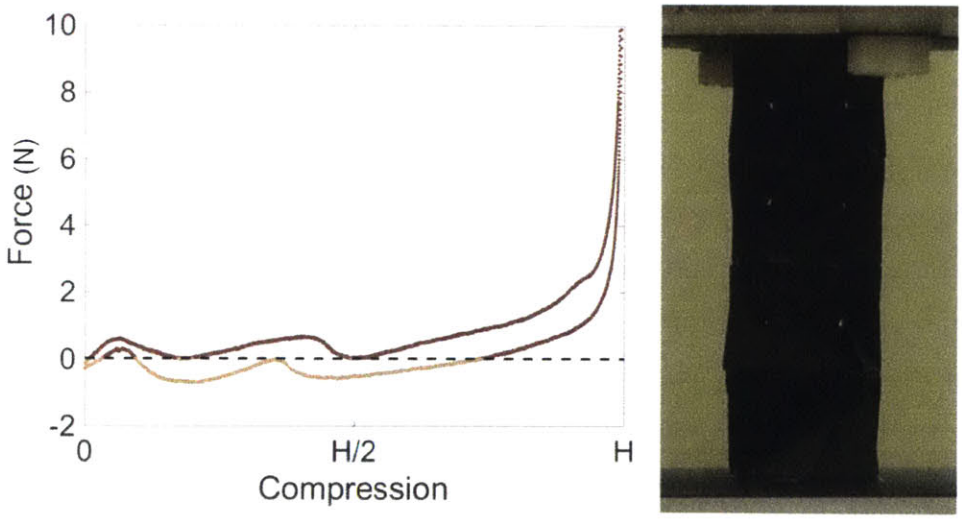

Figure 6-7: Force displacement response of four Flexigami cells of alternating chirality stacked in series and subjected to uniaxial compression tension tests when rotation of both the top and bottom platens is restricted

When these two kinds of towers are compressed in parallel keeping all the testing conditions same, we observe that effective force displacement response of the system to uni-axial compression is nothing but the sum of responses of individual towers.

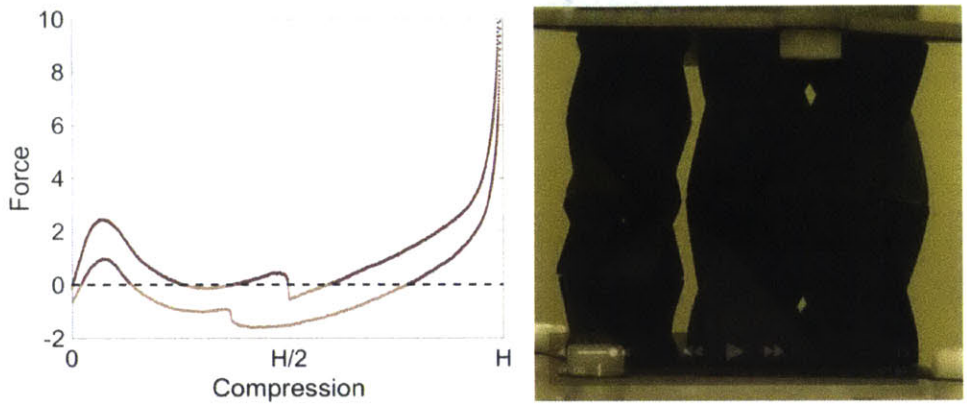

Figure 6-8: Force displacement response of two Flexigami towers with unit cells stacked in series are now placed parallel and subjected to uni-axial compression and tension tests with both the top and bottom platens restricted from rotating. We observe that the force displacement response is sum of responses of individual towers.

6.3 Mechanisms

One of the several applications of stacked *Flexigami* unit cells is their ability to be stored compactly and be deployed to cover very large distances. As explained before, because of the kinematic coupling between different geometrical quantities, axial compression of a unit cells results in the rotation of the top surface when the bottom surface is fixed. Turning this around, by providing a torque input to the bottom surface of *Flexigami* and preventing the top surface to rotate, results in the deployment of *Flexigami*. This is precisely demonstrated in Figure. 6-9. The single tube structure is created by combining stacked six-sided Flexigami unit cells with bellow structure made out of single sheet. Stacked Flexigami cells are placed concentrically and glued together at one end. Other end of the bellows is held constant. Figure 6-9 represents a completely stowed configuration. Rotating free end of *Flexigami* results in the sequential opening of its constituent unit cells and thus deployment of bellows.

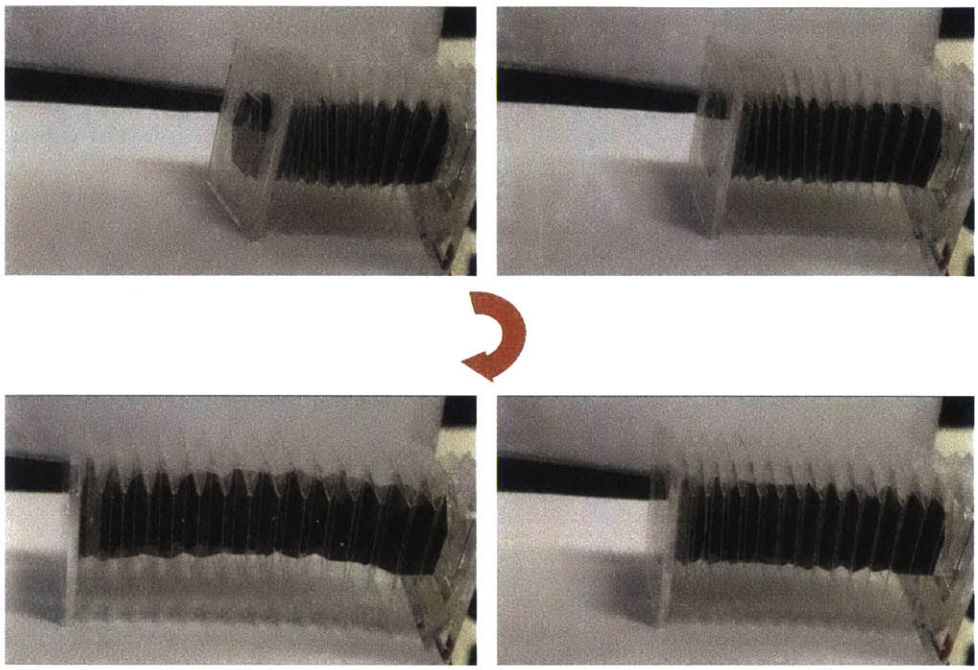

Figure 6-9: Photographs representing working principle of Flexigami mechanisms

Figure 6-9 represents the completely deployed configuration. Mechanics of individual components of this structure can be tuned to achieve fine control of its stiffness and thus its deployability. Our study of *Flexigami* introduces a novel collapsible cellular material and associated mechanisms. We discussed its unique mechanical properties and understood the contribution of individual structural components in shaping the overall response of a unit cell as well as different assemblies of these unit cells. This study highlights the effect of different boundary conditions on the response of a cellular assembly with net zero rotation. Extensions of this work may explore different cellular assemblies to result in huge structures which can be deployed at remote locations as well as refine the concepts presented in this article.

6.4 Summary

In this chapter we presented various configurations of *Flexigami* cells. First we explored two layer configurations where cells with opposite chirality as placed back to

back and subjected to different displacement boundary conditions on one of the two polygonal surfaces while the other is always held fixed. Depending on whether one of the surfaces is allowed to rotate freely or held fixed we obtained different force-displacement response. This provides initial data that force-displacement response of *Flexigami* cells can be engineered. As the next step, we stacked cells with varying λ in different possible combinations resulting in the same force-displacement response. A cell with lower stiffness will always be the first to get compressed to extended independent of its positioning in the arrangement. Tiling of cells in plane results in a response which is sum of responses of individual unit cells. Next, we present mechanisms possible with cellular assemblies of unit cells which provide basis to explore deployable structures.

THIS PAGE INTENTIONALLY LEFT BLANK

Chapter 7

Conclusions and Future Work

7.1 Conclusions

This thesis has explored the mechanics of *Flexigami* structures from understanding its geometric construction to developing deep insights into the role of material properties in defining the force-displacement responses of unit cells with different geometric configurations. In this work we modeled surfaces and creases with finite bending and crease rigidities which closely represent the properties of real materials as opposed to ideal assumption of rigid surfaces and perfect hinge behavior of creases. This is an important change from conventional method of understanding and modeling origami structures and forms back-bone of the current work. Imposed geometric constraints lead to interesting kinematic coupling between the tower height and rotation of the top surface when bottom is held fixed. These geometric constraints are fully satisfied only when the unit cell is fully opened or closed and thus forces the triangular panels to bend at any intermediate position to be able to satisfy these constraints. These deformations in the triangular panels are symmetric with respect to the total height of a unit cell and form the basis of observed bi-stable nature.

Numerical model of the *Flexigami* cell provides landscape of energy variations of the cell in a compression cycle. This model helps us understand the individual contributions of panel bending and crease folding to the total energy of the system. These individual contributions are dependent on the bending rigidity of panels and

rigidity of the creases. While crease energy is always monotonically increasing, panel bending offers an energy barrier. Careful tuning of these individual contributions has the ability to change the behavior of a unit cell from monostable to that of bistable. This proved to be an important tool in understanding the interplay between the two energy components and how they shape overall behavior of the unit cell.

While numerical modeling of *Flexigami* behavior is a great tool for parametric analysis of total energy variations in the system as well as individual contributions from panel bending and crease folding, it falls short in determining the actual stresses and strains developed in the structure in a compression cycle. To bridge this gap, we performed finite-element analysis of one particular case when $N = 7$, $L = 30$mm and $\lambda = 0.8$. It is found that stresses and strains developed in the triangular panels are small compared to the values along the creases. This is in agreement with the assumption of developable surfaces used in numerical model. Material model used in the FEM is obtained by characterizing the paper used in experimental sample preparation. Though this characterization suffices in determining bending rigidity of the panels, crease rigidity is yet to be found out with certainty and will be dealt in the future work.

The work detailed in this thesis provides a basis and furthers the use of available tools in understanding the mechanical responses of origami structures and modeling their behavior as structures fabricated from real material with finite thickness and anisotropic material properties. Moving forward, combination of finite-element tools along with numerical modeling sets a stage for analysis of other complex origami structures.

7.2 Future work

Origami as a tool to engineer functional structures and materials with interesting macroscopic mechanical properties has gained interest in the recent past. Many findings and applications of origami structures have been demonstrated. This thesis attempts to understand one such unit cell of a novel origami construction which we

call *Flexigami*. Some key questions have to be addressed and well understood before full potential of *Flexigami* as a unit cell of cellular materialcan be realized.

- Initial results of tuning of force-displacement curve as a result of different configurations of *Flexigami* cellular assemblies are demonstrated in Chapter 6. These results provide a promising start point for answering some of the important questions:
  - Can stiffness of each of the creases and panels be individually tuned to provide greater flexibility in tuning the mechanics of a unit cell?
  - Can assemblies of such unit cells with varying geometrical and mechanical properties be created in a methodical way to meet user defined requirements of its mechanical response?
  - Can any polynomial curve passing through the origin be recreated as force-displacement response of *Flexigami* cellular assembly?
- How does a *Flexigami* cell behave under dynamic loading conditions of varying frequency and amplitude? Especially oscillation of *Flexigami* around the point of instability might provide us with great insights into some of the important characteristics.

THIS PAGE INTENTIONALLY LEFT BLANK

Bibliography

[1] Abaqus documentation. *Dassault Systems, Providence, RI, USA.*

[2] Katia Bertoldi, Pedro M. Reis, Stephen Willshaw, and Tom Mullin. Negative poisson's ratio behavior induced by an elastic instability. *Advanced Materials*, 22(3):361–366, 2010.

[3] Nadia G Cheng, Arvind Gopinath, Lifeng Wang, Karl Iagnemma, and Anette E Hosoi. Thermally Tunable , Self-Healing Composites for Soft Robotic Applications a. pages 1–6, 2014.

[4] Marcelo a Dias. Swelling and folding as mechanisms of 3d shape formation in thin elastic sheets. *Ph.D. Thesis, University of Massachusetts Amherst*, (September).

[5] Marcelo a. Dias, Levi H. Dudte, L. Mahadevan, and Christian D. Santangelo. Geometric mechanics of curved crease origami. *Physical Review Letters*, 109:1–8, 2012.

[6] S. Felton, M. Tolley, E. Demaine, D. Rus, and R. Wood. A method for building self-folding machines. *Science*, 345(i):644–646, 2014.

[7] Bastiaan Florijn, Corentin Coulais, and Martin Van Hecke. Programmable mechanical metamaterials. *Physical Review Letters*, 175503, 2014.

[8] J.M. Gattas and Z. You. Geometric assembly of rigid-foldable morphing sandwich structures. *Engineering Structures*, 94:149–159, 2015.

[9] S. D. Guest and S. Pellegrino. The Folding of Triangulated Cylinders, Part I: Geometric Considerations. *Journal of Applied Mechanics*, 61(December 1994):773, 1994.

[10] S. D. Guest and S. Pellegrino. The Folding of Triangulated Cylinders, Part II: The Folding Process. *Journal of Applied Mechanics*, 61(December 1994):778, 1994.

[11] Cai Jianguo, Deng Xiaowei, Zhou Ya, Feng Jian, and Tu Yongming. Bistable Behavior of the Cylindrical Origami Structure With Kresling Pattern. *Journal of Mechanical Design*, 137(6):061406, 2015.

[12] By Arnaud Lazarus and Pedro M Reis. Soft Actuation of Structured Cylinders through Auxetic Behavior. *Advanced Engineering Materials*, (c):815–820.

[13] F. Lechenault, B. Thiria, and M. Adda-Bedia. Mechanical response of a creased sheet. *Physical Review Letters*, 112(24):1–5, 2014.

[14] Ying Liu, Julie K. Boyles, Jan Genzer, and Michael D. Dickey. Self-folding of polymer sheets using local light absorption. *Soft Matter*, 8(6):1764, 2012.

[15] A. E. F. Love. A treatise on the mathematical theory of elasticity.

[16] Ramses V. Martinez, Jamie L. Branch, Carina R. Fish, Lihua Jin, Robert F. Shepherd, Rui M D Nunes, Zhigang Suo, and George M. Whitesides. Robotic tentacles with three-dimensional mobility based on flexible elastomers. *Advanced Materials*, 25:205–212, 2013.

[17] Jiuke Mu, Chengyi Hou, Hongzhi Wang, Yaogang Li, Qinghong Zhang, and Meifang Zhu. Origami-inspired active graphene-based paper for programmable instant self-folding walking devices. *Science Advances*, (November), 2015.

[18] T. Mullin, S. Deschanel, K. Bertoldi, and M. C. Boyce. Pattern transformation triggered by deformation. *Physical Review Letters*, 99(8):1–4, 2007.

[19] Jun-hee Na, Arthur a Evans, Jinhye Bae, Maria C Chiappelli, Christian D Santangelo, Robert J Lang, Thomas C Hull, and Ryan C Hayward. Programming Reversibly Self-Folding Origami with Micropatterned Photo-Crosslinkable Polymer Trilayers. *Advanced Materials*, pages 79–85, 2015.

[20] Taketoshi Nojima. Modelling of Folding Patterns in Flat Membranes and Cylinders by Using Origami. *JSME International Journal*, 45:1050–1056, 2000.

[21] Johannes T. B. Overvelde, Tamara Kloek, Jonas J. a. DâĂŹhaen, and Katia Bertoldi. Amplifying the response of soft actuators by harnessing snap-through instabilities. *Proceedings of the National Academy of Sciences*, 2015.

[22] Y Pomeau and B Audoly. Elasticity and geometry from hair curls to the nonlinear response of shells. *Oxford.*

[23] Daniela Rus and Michael T Tolley. Design , fabrication and control of soft robots. *Nature*, 521, 2015.

[24] M. Schenk, S.D. Guest, and G.J. McShane. Novel stacked folded cores for blast-resistant sandwich beams. *International Journal of Solids and Structures*, 51(25-26):4196–4214, 2014.

[25] M Schenk, S G Kerr, a M Smyth, and Simon D Guest. Inflatable Cylinders for Deployable Space Structures. *Transformables*, (September):1–6, 2013.

[26] Mark Schenk and Simon D Guest. Geometry of Miura-folded metamaterials. *Proceedings of the National Academy of Sciences of the United States of America*, 110(9):3276–81, 2013.

[27] Mark Schenk, Andrew D. Viquerat, Keith a. Seffen, and Simon D. Guest. Review of Inflatable Booms for Deployable Space Structures: Packing and Rigidization. *Journal of Spacecraft and Rockets*, 51(3):762–778, 2014.

[28] J. Shim, C. Perdigou, E. R. Chen, K. Bertoldi, and P. M. Reis. Buckling-induced encapsulation of structured elastic shells under pressure. *Proceedings of the National Academy of Sciences*, 109:5978–5983, 2012.

[29] Jongmin Shim, Sicong Shan, Andrej Košmrlj, Sung H. Kang, Elizabeth R. Chen, James C. Weaver, and Katia Bertoldi. Harnessing instabilities for design of soft reconfigurable auxetic/chiral materials. *Soft Matter*, 9(34):8198–8202, 2013.

[30] Jesse L Silverberg, Jun-hee Na, Arthur a Evans, Bin Liu, Thomas C Hull, Christian D Santangelo, Robert J Lang, Ryan C Hayward, and Itai Cohen. Origami structures with a critical transition to bistability arising from hidden degrees of freedom. *Nature Materials*, (March):1–5, 2015.

[31] Jesse L Silverberg, Jun-hee Na, Arthur a Evans, Bin Liu, Thomas C Hull, Christian D Santangelo, Robert J Lang, Ryan C Hayward, and Itai Cohen. Origami structures with a critical transition to bistability arising from hidden degrees of freedom. *Nature Materials*, (March):1–5, 2015.

[32] Tomohiro Tachi and Koryo Miura. Rigid foldable cylidnders and Cells. *Journal of the International Association for Shell and spatial Structures*, pages 3–8.

[33] A Viquerat, M Schenk, B Sanders, and V Lappas. Inflatable Rigidisable Mast For End-Of-Life Deorbiting System. *European Conference on Spacecraft Structures, Materials and Environmental Testing (SSMET)*, pages 1–10, 2014.

[34] Dian Yang, Bobak Mosadegh, Alar Ainla, Benjamin Lee, Fatemeh Khashai, Zhigang Suo, Katia Bertoldi, and George M Whitesides. Buckling of Elastomeric Beams Enables Actuation of Soft Machines. *Advanced Materials*, pages 1–5.

[35] Yihui Zhang, Zheng Yan, Kewang Nan, Dongqing Xiao, Yuhao Liu, Haiwen Luan, Haoran Fu, Xizhu Wang, Qinglin Yang, Jiechen Wang, Wen Ren, Hongzhi Si, Fei Liu, Lihen Yang, Hejun Li, Juntong Wang, Xuelin Guo, Hongying Luo, Liang Wang, Yonggang Huang, and John a. Rogers. A mechanically driven form of Kirigami as a route to 3D mesostructures in micro/nanomembranes. *Proceedings of the National Academy of Sciences*, 112(38):201515602, 2015.